JVI Journals.ASM.org

Entry of a Novel Marine DNA Virus, Singapore Grouper Iridovirus, into Host Cells Occurs via Clathrin-Mediated Endocytosis and Macropinocytosis in a pH-Dependent Manner

Shaowen Wang,[a,c] Xiaohong Huang,[a,c] Youhua Huang,[a,c] Xian Hao,[b] Haijiao Xu,[b] Mingjun Cai,[b] Hongda Wang,[b,c] Qiwei Qin[a,c]

Key Laboratory of Tropical Marine Bio-resources and Ecology, South China Sea Institute of Oceanology, Chinese Academy of Sciences, Guangzhou, China[a]; State Key Laboratory of Electroanalytical Chemistry, Changchun Institute of Applied Chemistry, Chinese Academy of Sciences, Changchun, China[b]; University of Chinese Academy of Sciences, Beijing, China[c]

ABSTRACT

Iridoviruses are nucleocytoplasmic DNA viruses which cause great economic losses in the aquaculture industry but also show significant threat to global biodiversity. However, a lack of host cells has resulted in poor progress in clarifying iridovirus behavior. We investigated the crucial events during virus entry using a combination of single-virus tracking and biochemical assays, based on the established virus-cell infection model for Singapore grouper iridovirus (SGIV). SGIV infection in host cells was strongly inhibited when cells were pretreated with drugs blocking clathrin-mediated endocytosis, including sucrose and chlorpromazine. Inhibition of key regulators of macropinocytosis, including Na^+/H^+ exchanger, Rac1 GTPase, p21-activated kinase 1 (PAK1), protein kinase C (PKC), and myosin II, significantly reduced SGIV uptake. Cy5-labeled SGIV particles were observed to colocalize with clathrin and macropinosomes. In contrast, disruption of cellular cholesterol by methyl-β-cyclodextrin and nystatin had no effect on virus infection, suggesting that SGIV entered grouper cells via the clathrin-mediated endocytic pathway and macropinocytosis but not via caveola-dependent endocytosis. Furthermore, inhibitors of endosome acidification such as chloroquine and bafilomycin A1 blocked virus infection, indicating that SGIV entered cells in a pH-dependent manner. In addition, SGIV particles were observed to be transported along both microtubules and actin filaments, and intracellular SGIV motility was remarkably impaired by depolymerization of microtubules or actin filaments. The results of this study for the first time demonstrate that not only the clathrin-dependent pathway but also macropinocytosis are involved in fish DNA enveloped virus entry, thus providing a convenient tactic for exploring the life cycle of DNA viruses.

IMPORTANCE

Virus entry into host cells is critically important for initiating infections and is usually recognized as an ideal target for the design of antiviral strategies. Iridoviruses are large DNA viruses which cause serious threats to ecological diversity and the aquaculture industry worldwide. However, the current understanding of iridovirus entry is limited and controversial. Singapore grouper iridovirus (SGIV) is a novel marine fish DNA virus which belongs to genus *Ranavirus*, family *Iridoviridae*. Here, using single-virus tracking technology in combination with biochemical assays, we investigated the crucial events during SGIV entry and demonstrated that SGIV entered grouper cells via the clathrin-mediated endocytic pathway in a pH-dependent manner but not via caveola-dependent endocytosis. Furthermore, we propose for the first time that macropinocytosis is involved in iridovirus entry. Together, this work not only contributes greatly to understating iridovirus pathogenesis but also provides an ideal model for exploring the behavior of DNA viruses in living cells.

Viruses have developed a "Trojan horse" strategy to overcome barriers to their successful infection of host cells (1, 2). Viral infection is initiated by contact between the virus and the cell membrane, finally resulting in virus transport to an intracellular replication site for gene expression (3). Knowledge of how viruses break through the host cell membrane is necessary to further our understanding of virology and cell biology and to improve antiviral drug design. Early studies relied mainly on electron microscopy and biochemical assays; however, a single-virus tracking technique in living cells with high temporal and spatial resolutions in real time has recently provided a powerful tool for elucidating the dynamic events occurring during natural and artificial virus-cell interactions (1, 2, 4). The pathways followed by viruses on their way into and through cells can be observed directly, thus substantially improving our understanding of viral entry.

Numerous viruses hijack cellular endocytic pathways of entry, including clathrin-dependent endocytosis, lipid raft/caveola-dependent and non-clathrin-lipid raft/caveola-dependent pathways, and macropinocytosis (2, 4–6). Clathrin-mediated endocytosis is a classical endocytic pathway which most viruses use as the primary means of internalization (7–10). During this process, clathrin is assembled on the plasma membrane to form a coated

Received 18 June 2014 Accepted 25 August 2014
Published ahead of print 27 August 2014
Editor: G. McFadden
Address correspondence to Hongda Wang, hdwang@ciac.ac.cn, or Qiwei Qin, qinqw@scsio.ac.cn.
S.W. and X.H. contributed equally to this article.
Supplemental material for this article may be found at http://dx.doi.org/10.1128/JVI.01744-14.

doi:10.1128/JVI.01744-14

pit (CCP), which then invaginates to form a clathrin-coated vesicle (CCV) containing the internalized cargo. The vesicle subsequently sheds its clathrin coat, followed by acidification and transportation. A series of essential molecules, including Eps15, dynamin, and adapter protein AP2, are involved in this pathway. In multicolor live-cell images, influenza virus and vesicular stomatitis virus (VSV) are shown to induce the *de novo* assembly of clathrin; in contrast, canine parvovirus and dengue virus diffuse into nascent and assembled CCPs (8, 11–14). The lipid raft/caveola-dependent entry route, which is used by many viruses, including simian virus 40 (SV40), human papillomavirus (HPV), and echovirus 1 (EV1), is generally characterized by high levels of cholesterol and sphingolipids (7). Caveolae, composed of caveolin, are flask-shaped invaginations of the plasma membrane, which is approximately 50 to 80 nm in size. Because caveolae are associated with cholesterol-rich membrane microdomains termed lipid rafts, disruption of membrane cholesterol severely inhibits lipid raft/caveola endocytosis-mediated virus entry. Compared with clathrin-mediated endocytosis, vesicles called caveosomes transport via a different route (7, 15, 16). Macropinocytosis has recently been a focus of attention (17); this is a means by which a growing number of viruses, such as vaccinia virus (VACV) (18), African swine fever virus (ASFV) (19), and adenovirus serotype 3 (20), have been found to enter cells and which is usually considered to be a non-receptor-dependent mechanism stimulated by external factors, such as growth factors and pathogens. Macropinocytosis induces membrane ruffles driven by actin polymerization underneath the membrane surface (21, 22). When a ruffle retracts, it forms large cytoplasmic vacuoles, called macropinosomes, that are up to several micrometers in diameter (23). Some signal factors, such as phosphoinositide 3-kinase (PI3K), Akt, and protein kinase C (PKC), act to promote membrane ruffling by stimulating actin rearrangement (24–26). For VACV strain Western Reserve (WR), virus binding to the cell body triggers dramatic and transient membrane blebbing mimicking apoptosis, and the virus enters the cell during bleb retraction. In contrast, the VACV strain International Health Department-J (IHD-J) induces filopodia on the host cells, rather than apoptotic mimicry (18, 27). Besides the endocytic pathways mentioned above, another pathway involving non-clathrin-lipid raft/caveola-dependent endocytosis also exists (28–30), though the details remain unclear.

Single-virus tracking provides an ideal method for monitoring virus movement. Several viruses, such as murine leukemia virus (MLV), VSV, and HPV, use the actin cytoskeleton beneath the membrane for direct movement along microvilli or filopodia to enter the cell body (31–33). Upon internalization, viruses such as VSV, influenza virus, Ebola virus (EBOV), and SV40, which enter via different endocytic pathways, are sorted to different endosomal compartments for efficient navigation and gene release (34–36). Viruses internalized via clathrin-dependent and caveola-dependent routes are initially delivered to early endosomes (EEs), then sorted into either recycling endosomes or late endosomes (LEs), and eventually fused with lysosomes (LYs) (2). Viruses entering via macropinocytosis are initially delivered to macropinosomes and subsequently follow a similar route. The Rab small GTPases coordinate vesicular transport and determine endocytic vesicle specificity, so they are important tools to study endosome trafficking (37). Rab5 is necessary to EEs, while Rab7 is located primarily on LEs and regulates the function of LEs (38, 39).

Several viruses move along actin or microtubules using a molecular motor, which functions as an active transporter in the crowded cytoplasm (2). Because the cell interior consists of a densely packed network of organelles, macromolecules, and cytoskeletal components, objects with molecular of masses >500 kDa cannot diffuse freely within the cytoplasm and require active cellular transport, such as by endocytosis, membrane trafficking, and cytokinesis (4, 40). Many viruses transport along microtubules by motor proteins, as observed for influenza virus, human immunodeficiency virus (HIV), and adeno-associated virus serotype 2 (11, 41–43), while poliovirus (PV) and the surface antigen of hepatitis B virus (HBsAg) have been clearly shown to transport rapidly along actin (4, 44).

Iridoviruses, members of nucleocytoplasmic large DNA viruses (NCLDV), not only cause great economic losses in the aquaculture industry but also are emerging infectious disease agents showing a significant threat to global biodiversity (45, 46). To our knowledge, iridoviruses are capable of infecting invertebrates and poikilothermic vertebrates, such as insects, fish, amphibians, and reptiles (45, 47), implying that the iridoviruses can be used as an ideal virus model to investigate virus behavior conveniently and safely in living cells. However, the molecular mechanism underlying iridovirus entry into cells is poorly understood due to the lack of host cells (45). A type species of the genus *Ranavirus*, frog virus 3 (FV3), enters into mammalian cells by clathrin-mediated endocytosis (48). In contrast, recent studies on tiger frog virus (TFV) (a ranavirus) and infectious spleen and kidney necrosis virus (ISKNV) (a megalocytivirus) demonstrate that both of them enter cells via caveola-dependent endocytosis but not clathrin-mediated endocytosis (16, 49). Singapore grouper iridovirus (SGIV) was first isolated from diseased grouper (*Epinephelus tauvina*) and characterized as a novel member of the genus *Ranavirus*, family *Iridoviridae* (50). SGIV infection induces a highly lethal and serious systemic disease in the grouper industry, often resulting in significant economic losses (50, 51). Despite extensive research into virus genomics (52), transcriptomics (53, 54), and proteomics (55), as well as the molecular mechanism of SGIV-induced cell death (56), the crucial events occurring during SGIV entry remain largely unknown, except for some evidence from electron microscopy (50).

In this study, we examined the process of SGIV infection using biochemical assays and single-particle tracking to detect the dynamic and multiple entry pathways of SGIV. Our results not only contribute greatly to understanding iridovirus pathogenesis but also provide new insights into exploring the natural entry mechanisms of NCLDV in lower vertebrates.

MATERIALS AND METHODS

Cell and viruses. The grouper spleen (GS) cell line used in this study was established in our previous study (57). Cells were cultivated and maintained in Leibovitz's L-15 medium containing 10% fetal bovine serum (Gibco) at 28°C. For live-cell fluorescence imaging, GS cells were cultured for 18 or 24 h to achieve 75% confluence in 35-mm glass-bottom culture dishes. Cells were washed with serum-free, phenol red-free medium prior to fluorescence experiments and were maintained in this medium for confocal imaging and real-time experiments. For biochemical analysis and immunofluorescence assay (IFA), GS cells were seeded on coverslips in 6-well plates or cultured in 24-well plates for 18 or 24 h to achieve 75% confluence.

The SGIV used in this study was originally isolated from diseased grouper (*E. tauvina*) (50). SGIV was propagated in GS cells, and virus stocks were maintained at −80°C.

Reagents. Chlorpromazine (CPZ), sucrose, dynasore, methyl-β-cyclodextrin (MβCD), nystatin, ethyl-isopropyl amiloride (EIPA), chloroquine (CQ), bafilomycin A1 (Baf A1), cytochalasin D (Cyto D), and nocodazole were purchased from Sigma-Aldrich. All drugs, except CPZ, sucrose, and MβCD were dissolved in dimethyl sulfoxide (DMSO) according to the manufacturer's instructions. The lipophilic dye DiO and amine-reactive Cy5 were purchased from Biotium. Alexa Fluor 488 phalloidin and LysoTracker were obtained from Invitrogen, and fluorescein isothiocyanate (FITC)-dextran (10 kDa) was purchased from Sigma. In addition, the plasmids pEGFP-Rab7, pEGFP-Rab5, pEGFP-tub, and pEGFP-CLa used in this study were kept in our lab.

Virus purification and fluorescence labeling. Virus purification was carried out as described previously (50). Briefly, SGIV was inoculated onto confluent monolayers of GS cells at a multiplicity of infection of approximately 0.1. When the cytopathic effect was sufficient, the medium containing SGIV was harvested, followed by three cycles of rapid freezing and thawing. The medium was then centrifuged at 12,000 × *g* (Eppendorf 5810R centrifuge) for 30 min at 4°C. The supernatant was centrifuged at 200,000 × *g* (Beckman 70 Ti rotor) for 1 h at 4°C, and the pellet was resuspended in TN buffer (50 mM Tris-HCl, 150 mM NaCl, pH 7.5), layered onto a gradient of 30 to 60% (wt/vol) sucrose, and centrifuged at 150,000 × *g* (Beckman SW 40 rotor) for 1 h at 4°C. The resulting virus bands were collected and diluted with TN buffer. Virion pellets were washed by centrifugation at 100,000 × *g* for 1 h at 4°C, collected and suspended in TN buffer, and then stored at −80°C until use. SGIV particles were examined by transmission electron microscopy and labeled with Cy5 by incubating SGIV stock solution with dye in phosphate-buffered saline (PBS) (pH 7.4) at room temperature for 2 h with gentle vortexing. Unincorporated dye was removed by three high-speed centrifugations at 14,000 × *g* (Eppendorf 5810R centrifuge) at 4°C for 60 min. Immediately before experiments, viral aggregates were removed by passage through 0.2-μm-pore-size filters (Supor membrane; Pall) and examined under transmission electron microscopy.

Cell transfection. GS cells grown to 70% confluence were transiently transfected with plasmids using the X-tremeGENE HP DNA transfection reagent (Roche) according to the manufacturer's instructions. In brief, 1 to 2 μg of plasmid and 2 to 4 μl of transfection reagent were mixed in L-15 medium and then incubated with GS cells. After another 24 h of culture, the fluorescence was observed under confocal laser scanning microscopy (CLSM) for further studies.

Kinetics of SGIV infection. GS cells were incubated with SGIV for 0, 1, 2, 3, 4, 5, 6, 7, or 8 h at 28°C. Citrate buffer (40 mM sodium citrate, 10 mM KCl, and 135 mM NaCl, pH 3.1) was added and left for 45 s to inactivate and remove noninternalized viruses. Cells were examined at 48 h postinfection (hpi) by IFA using anti-VP19 antibody (58).

Kinetics of SGIV entry. GS cells were prechilled at 4°C for 30 min and exposed to SGIV for 30 min at 4°C for virus binding. The cells were then washed with precooling medium before addition of fresh medium. Noninternalized viruses were inactivated and removed with citrate buffer at 0, 0.5, 1, 1.5, 2, 2.5, 3, 3.5, and 4 h after a shift to 28°C. The cells were collected at 36 hpi for IFA.

SGIV uptake and infection assays. To analyze SGIV uptake, GS cells were pretreated with the inhibitors listed above (except for Cyto D and nocodazole) in serum-free medium at 28°C for 2 h. SGIV was then added to the medium in the presence of the drugs and left for 2 h at 28°C. Cells were either washed twice with medium and fixed with 4% paraformaldehyde for further analysis by CLSM or washed once with citrate buffer to remove noninternalized viruses and harvested at 48 hpi to prepare for IFA or Western blotting.

For tracking experiments, cells were incubated in medium containing Cyto D for 60 min or in medium containing nocodazole for 120 min to disrupt actin filaments or microtubules, respectively, prior to infection. Image acquisition was performed in the presence of drugs during all experiments.

Fluorescence microscopy and real-time virus tracking assay. Fluorescent images were obtained through a Leica TCS SP2 confocal microscope. Cy5-labeled SGIV particles were excited with a 633-nm helium-neon laser, and DiO, enhanced green fluorescent protein (EGFP), Alexa Fluor 488 phalloidin, FITC-dextran, and LysoTracker were excited with a 488-nm Ar-Kr laser. A custom-designed polychroic beam splitter that reflected at 650 to 680 and 500 to 530 nm was used to direct the laser lines onto the samples, respectively. Fluorescence emission was collected and imaged through a 100× oil immersion objective with a numerical aperture of 1.4. Experiments were conducted at 28°C. For real-time tracking, two-color live-cell fluorescence imaging was performed, and image series were recorded at a frequency of several seconds per frame. The motility of viruses and colocalization of viruses with various cellular structures were analyzed using Image-Pro Plus 6.0 and MATLAB.

Western blotting. Cells were harvested and lysed in PBS containing 1× sodium dodecyl sulfate (SDS) loading buffer. The protein concentration was measured using a Bradford protein assay kit. Cell lysates were fractionated by SDS-polyacrylamide gel electrophoresis and transferred to polyvinylidene fluoride membranes for 70 min. The separated proteins were reacted with anti-VP19 as the primary antibody, at a dilution of 1:1,000. The secondary antibody was horseradish peroxidase–goat anti-mouse antibody at a dilution of 1:1,000. Internal control reactions to detect β-actin were carried out simultaneously. Immunoblots were visualized using an enhanced chemiluminescence detection system according to the manufacturer's protocol (Amersham ECL Western blotting detection kit). Data were obtained from three independent experiments.

Immunofluorescence microscopy. Cells were fixed with 4% paraformaldehyde, permeabilized with 0.2% Triton X-100 for 15 min, and blocked with bovine serum albumin (BSA) (Sigma). Cells were then washed three times with PBS and incubated with primary antibodies against VP19 (1:100) diluted in 0.2% BSA at room temperature for 2 h. After washing, fluorescence isothiocyanate-conjugated goat anti-mouse IgG was added and left at room temperature for 2 h. Cells were imaged under an inverted fluorescence microscope (Zeiss, Germany).

RESULTS

Dynamics of SGIV entry into GS cells. Virus infection and entry kinetics were determined in GS cells. The percentage of SGIV infection of GS cells initially increased rapidly, reaching the half-maximal level (50%) at 30 min, and plateaued after 2 h (Fig. 1A). Analysis of SGIV entry consistently indicated that most SGIV viral particles entered GS cells at 1 hpi (Fig. 1B), suggesting that SGIV entry is relatively rapid compared with those of TFV and ISKNV (16, 49).

To detect the course of SGIV entry visually, SGIV particles were labeled with fluorescent dye and individual virus particles were tracked by CLSM. Using Cy5-*N*-hydroxysuccinimide, which could spontaneously insert into the viral capsid, we found that Cy5-labeled SGIV-infected GS cells as well as wild-type SGIV particles (data not shown). After incubation with Cy5-labeled SGIV at 4°C for 30 min, cells were plated rapidly at 28°C to initiate infection. Cells were fixed for observation at the indicated time points (0, 30, 60, and 120 min). As shown in Fig. 1C, SGIV virus particles bound to the cell plasma membrane without endocytosis at 4°C, and infection was rapidly initiated when the temperature was increased to 28°C, followed by a time-dependent increase in virus particles in the cytoplasm with increasing infection time (Fig. 1D to F). The number of virus particles remained similar between 1.5 and 6 hpi (data not shown), suggesting that SGIV entry was complete by 120 min after infection.

Several viruses rely on retrograde transport of actin-rich filopodia before becoming internalized (31–33). We recorded and analyzed the actions of single Cy5-labeled SGIV particles. SGIVs

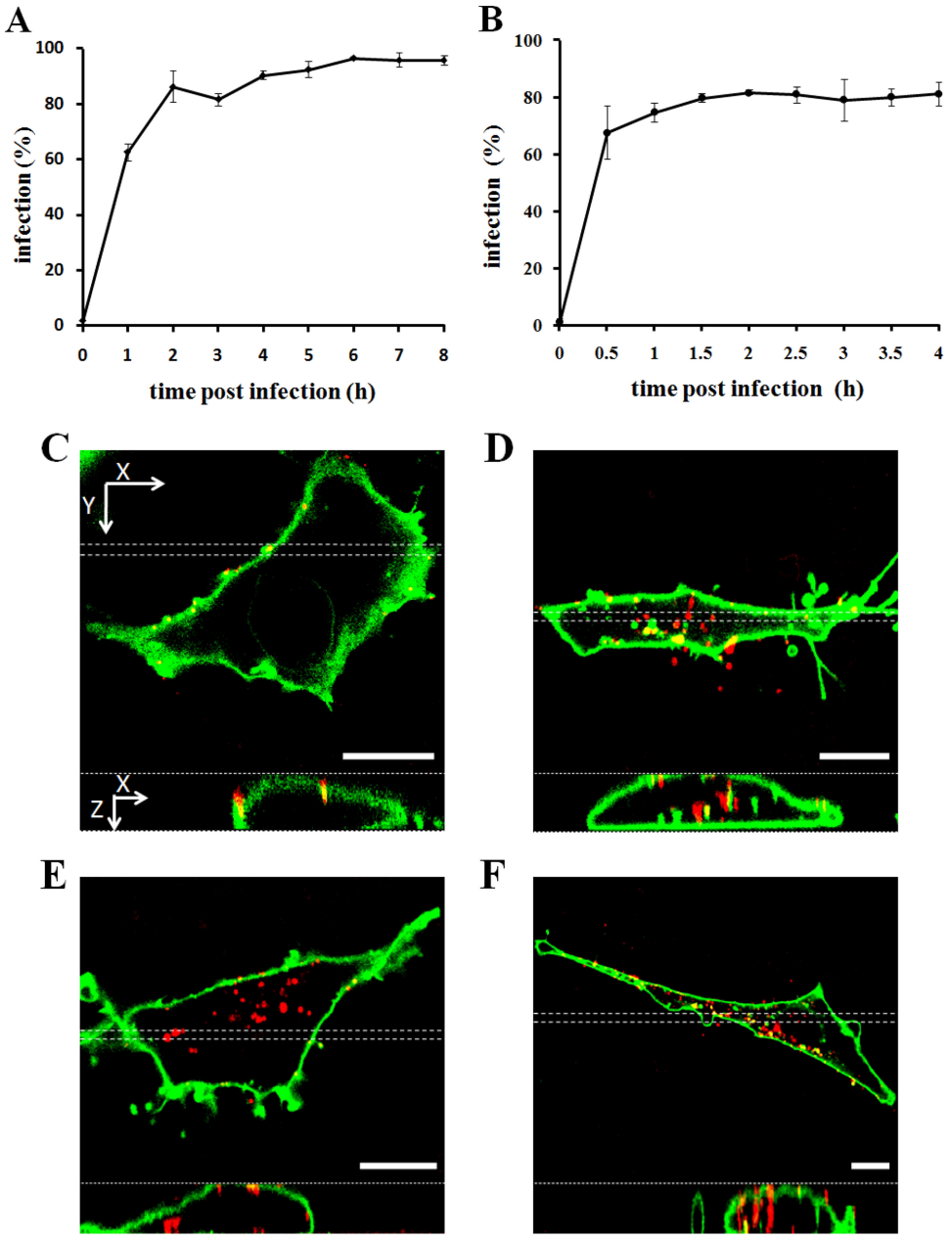

FIG 1 Course of SGIV infection in GS cells. (A) Infection kinetics of SGIV. GS cells were incubated with SGIV, and noninternalized SGIVs were inactivated with citrate buffer at the indicated time points. The infectivity was calculated by IFA at 48 hpi using anti-VP19 antibody. (B) Entry kinetics of SGIV. Viral adsorption to cells was performed at 4°C, viruses were washed twice with medium to remove unbound viruses, and then the temperature was shifted to 28°C to stimulate infection. Noninternalized SGIVs were inactivated with citrate buffer at the indicated times. The infection rate was calculated by IFA at 36 hpi. (C to F) Three-dimensional (3D) confocal images of GS cells at different times postinfection. GS cells were infected by Cy5-labeled SGIV (red) and immobilized at 0 min (C), 30 min (D), 60 min (E), and 120 min (F) after infection. Just before imaging, GS cells were incubated with DiO to show the cell boundaries (green). Successive z-stacks spaced by 200 nm were recorded to construct the 3D images. The *xz* image plane used for recording in all experiments was approximately 1 μm thick, as indicated by the dashed lines. Scale bars are 10 μm.

traveled along filopodia-like protrusions to reach the surface of the cell body and then moved from the cell membrane toward the intracellular environment (Fig. 2A; see Movie S1 in the supplemental material). Meanwhile, individual SGIV particles attached to the protrusion arrived at the cell surface as the protrusion retracted (Fig. 2B; see Movie S2 in the supplemental material).

Clathrin-mediated endocytosis is involved in SGIV entry. To determine the role of clathrin-mediated endocytosis in SGIV entry, we blocked clathrin-dependent endocytosis using CPZ and sucrose. CPZ can prevent the assembly of coated pits at the cell surface and can induce clathrin lattices to assemble on endosomal membranes, while hypertonic sucrose can disturb the formation of CCVs on the cell membrane, thereby hindering clathrin-dependent endocytosis (59). Confocal images revealed a noticeable reduction in Cy5-labeled SGIV particles entering cells treated with 20 μM CPZ compared with mock-treated cells (Fig. 3A). We pre-

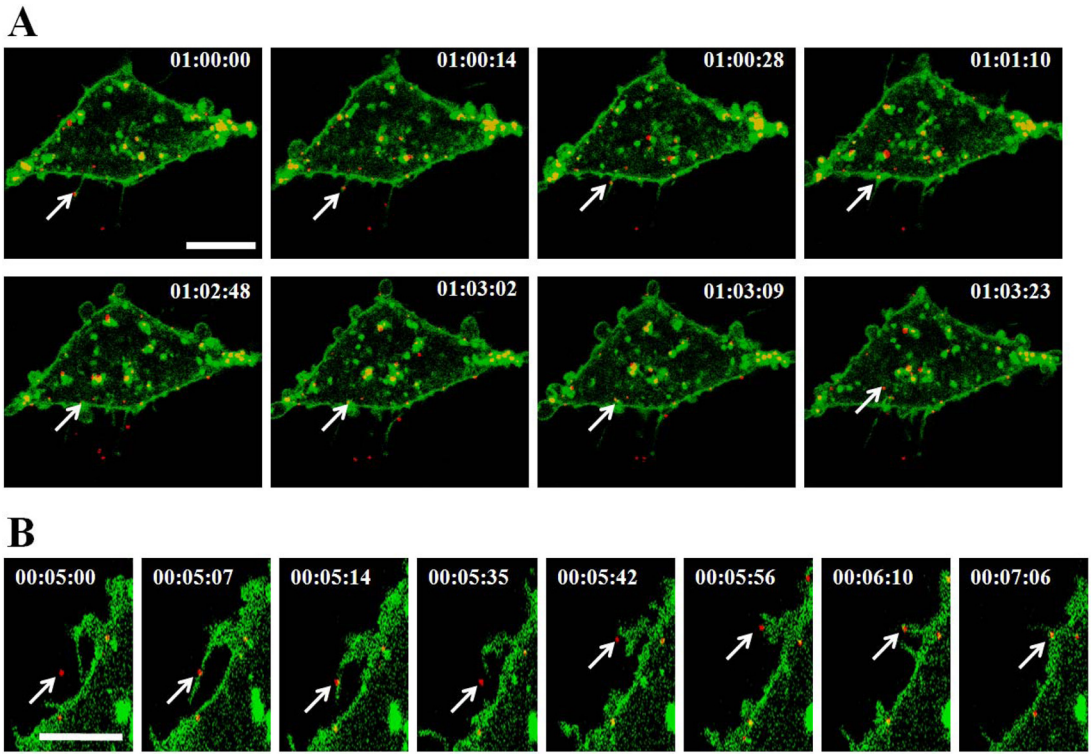

FIG 2 Dynamics of individual SGIV entry into GS cell. (A) SGIV transports along filopodia-like protrusions and then enters into the cell. GS cells labeled with DiO (green) were incubated with Cy5-labeled SGIV (red), and the dynamic SGIV-cell interaction was visualized by CLSM. The arrows indicate an individual SGIV particle surfing along the protrusion, reaching the cell surface, and moving into the cytoplasm. (B) Retraction of surface protrusions serves as another means of transferring SGIV to the cell surface. The arrows show an individual SGIV particle retracting with the gradually shortening protrusion to arrive at the cell surface. Scale bars are 10 μm.

viously demonstrated that SGIV VP19 was an envelope protein that could be specifically recognized by antibody against VP19 during SGIV infection (58). In the present study, we also assessed the percentage of SGIV-infected cells under treatment with different drugs using IFA. Fluorescent signaling was obviously reduced in the presence of CPZ (Fig. 3B), and the percentage of SGIV was significantly decreased to 21% (Fig. 3C). Viral protein synthesis was determined by Western blotting. CPZ greatly inhibited viral protein synthesis compared with that for untreated controls (Fig. 3C), while 300 μM sucrose also significantly decreased the percentage of SGIV-infected cells and VP19 protein synthesis (Fig. 3D). The effects of both CPZ and sucrose on SGIV entry were dose dependent.

Dynamin is an essential cellular GTPase involved in cellular membrane fission during vesicle formation. It exerts vital roles in clathrin-dependent and lipid raft/caveola-dependent endocytic pathways (7). We therefore validated the role of dynamin in SGIV entry using dynasore, which rapidly and specifically inhibits the GTPase activity of dynamin (60). The percentage of SGIV-infected cells decreased significantly in the presence of dynasore, in a dose-dependent manner (Fig. 3E). Viral structural protein synthesis and SGIV particles were obviously reduced in SGIV-infected dynasore-treated cells (Fig. 3A and E). Furthermore, to determine if SGIV virus particles were associated with clathrin, GS cells were transfected with pEGFP-LCa to indicate clathrin, and after SGIV infection, some virus particles colocalized with clathrin clusters (Fig. 3F). Together, these results establish that dynamin-dependent and clathrin-mediated endocytosis is involved in SGIV entry.

Entry of SGIV is independent of lipid raft/caveolin. Iridoviruses, including TFV and ISKNV, enter cells via caveola-dependent endocytosis (16, 49). We therefore investigated whether lipid raft/caveola-dependent endocytosis was also involved in SGIV infection. MβCD disrupts cholesterol-rich microdomains, while nystatin is a sterol-binding drug (61, 62), and both MβCD and nystatin can therefore block the lipid raft/caveola-dependent endocytic pathway. Cells were pretreated with various concentrations of MβCD or nystatin and incubated with Cy5-labeled SGIV for 120 min. Samples were then examined by CLSM. There were no obvious differences in SGIV uptake among MβCD, nystatin-treated, or mock-treated cells (Fig. 4A). Furthermore, SGIV infectivity was unaffected by MβCD or nystatin treatment ($P > 0.05$), even at the highest concentrations, and neither MβCD nor nystatin had any effect on viral protein synthesis (Fig. 4B and C). These results reveal that cell entry of SGIV is independent of lipid raft/caveolin-dependent endocytosis.

SGIV uses macropinocytosis to enter host cells. Apart from the clathrin- and caveolin-mediated endocytotic processes, macropinocytosis is a unique mode of endocytosis that has received increasing attention because of its roles in immune defense and virus entry (17, 63). Numerous reports have demonstrated that macropinocytosis is an important alternate route for the cellular entry of mammalian viruses; however, its role in DNA virus infection of lower vertebrates remains largely unknown. We used the

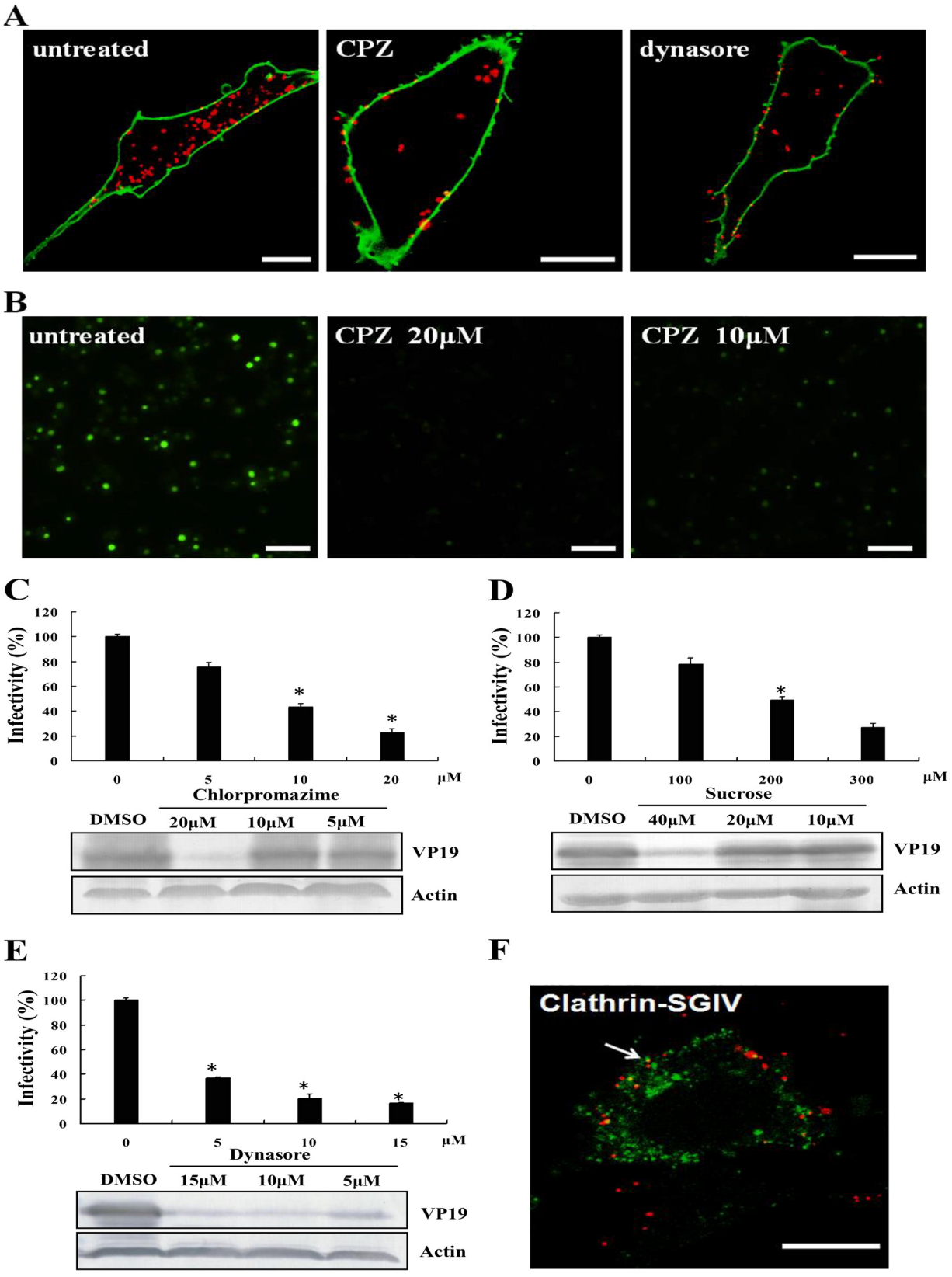

FIG 3 SGIV entry depends on clathrin-mediated endocytosis and dynamin. (A) CPZ and dynasore inhibit SGIV uptake. GS cells were pretreated with CPZ or dynasore for 120 min, or were left untreated, and then were incubated with Cy5-labeled SGIV (red) for 120 min. Infected cells were labeled with DiO (green), and more than 100 cells were analyzed by CLSM. (B) Detection of VP19 expression in mock-treated or CPZ-treated cells by immunostaining. Cells were pretreated with different amounts of CPZ for 120 min and infected with SGIV. The infected cells were then analyzed at 48 hpi by IFA using anti-VP19 antibody (green). (C

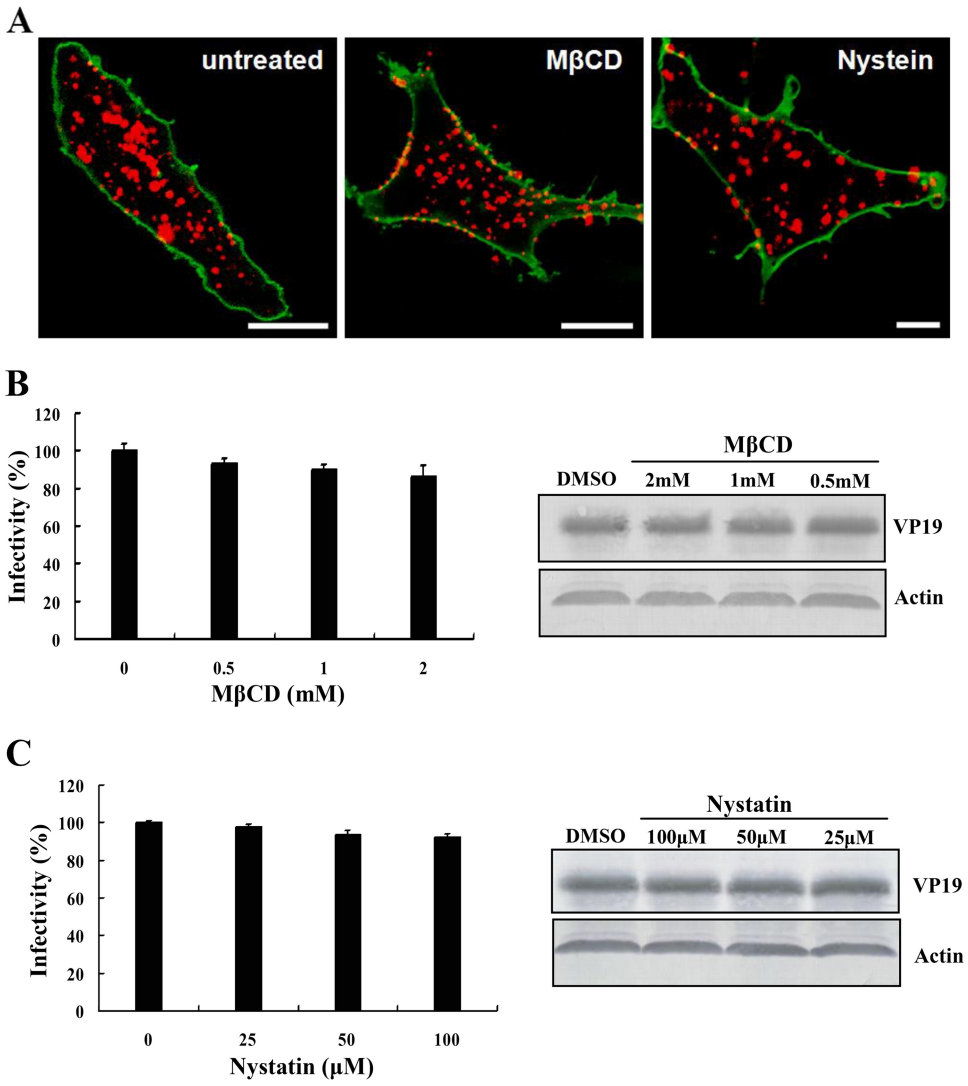

FIG 4 Inhibition of caveolin-mediated endocytosis does not block SGIV entry. (A) MβCD and nystatin do not inhibit SGIV uptake. GS cells were pretreated with various concentrations of MβCD or nystatin, followed by infection with Cy5-labeled SGIV (red) for 120 min. After the infected cells were labeled with DiO (green), more than 100 cells were examined by CLSM. (B and C) MβCD (B) and nystatin (C) have no influence on SGIV infectivity or viral protein synthesis. GS cells were pretreated with different concentrations of MβCD or nystatin for 120 min and then incubated with SGIV for 120 min. After being washed with citrate buffer to remove noninternalized viruses, the cells were harvested at 48 hpi. Infectivity was examined by IFA, and the level of infection of the treated cells was normalized to that of the untreated cells. The results are from triplicate experiments, and error bars indicate the means ± SD. The levels of SGIV viral protein and β-actin were analyzed by Western blotting. Scale bars are 10 μm. *, $P < 0.05$.

Na^+/H^+ exchanger inhibitor EIPA, which specifically inhibits macropinocytosis, to clarify the role of macropinocytosis in SGIV entry. Treatment with 40 μM EIPA reduced the uptake of fluorescently labeled SGIV particles in the cytoplasm (Fig. 5A). Moreover, IFA showed that the percentage of SGIV-infected cells was significantly reduced in the presence of 20 μM or 40 μM EIPA, compared with mock-treated cells ($P < 0.05$), suggesting that SGIV entry depended on the Na^+/H^+ exchanger (Fig. 5B and C). Viral protein synthesis was also significantly reduced by treatment with EIPA. Furthermore, some virus particles colocalized with the fluid-phase marker dextran, which could indicate macropinosomes (Fig. 5D).

Increasing numbers of studies have reported signaling events during the macropinocytic mechanism of endocytosis, especially

to E) SGIV infectivity and viral protein synthesis are impaired by CPZ (C), sucrose (D), and dynasore (E). GS cells were pretreated with different drugs at the indicated concentrations for 120 min and were then infected with SGIV for 120 min. After being washed in citrate buffer to remove noninternalized viruses, the cells were collected at 48 hpi. The infection rate was examined by IFA and was quantified as the percentage of treated cells with incorporated viruses relative to that for untreated cells. The viral infection rate of untreated cells was arbitrarily set as 100%. The data shown are the means and standard deviations (SD) of the results from three independent experiments. Endogenous β-actin was used as an internal loading control for Western blotting. (F) SGIV particles colocalize with clathrin. GS cells were transfected with pEGFP-LCa prior to incubation with Cy5-labeled SGIVs. The arrow indicates an individual SGIV particle (red) colocalized with clathrin (green). Scale bars are 10 μm (A and F) and 50 μm (B). *, $P < 0.05$. DMSO, dimethyl sulfoxide.

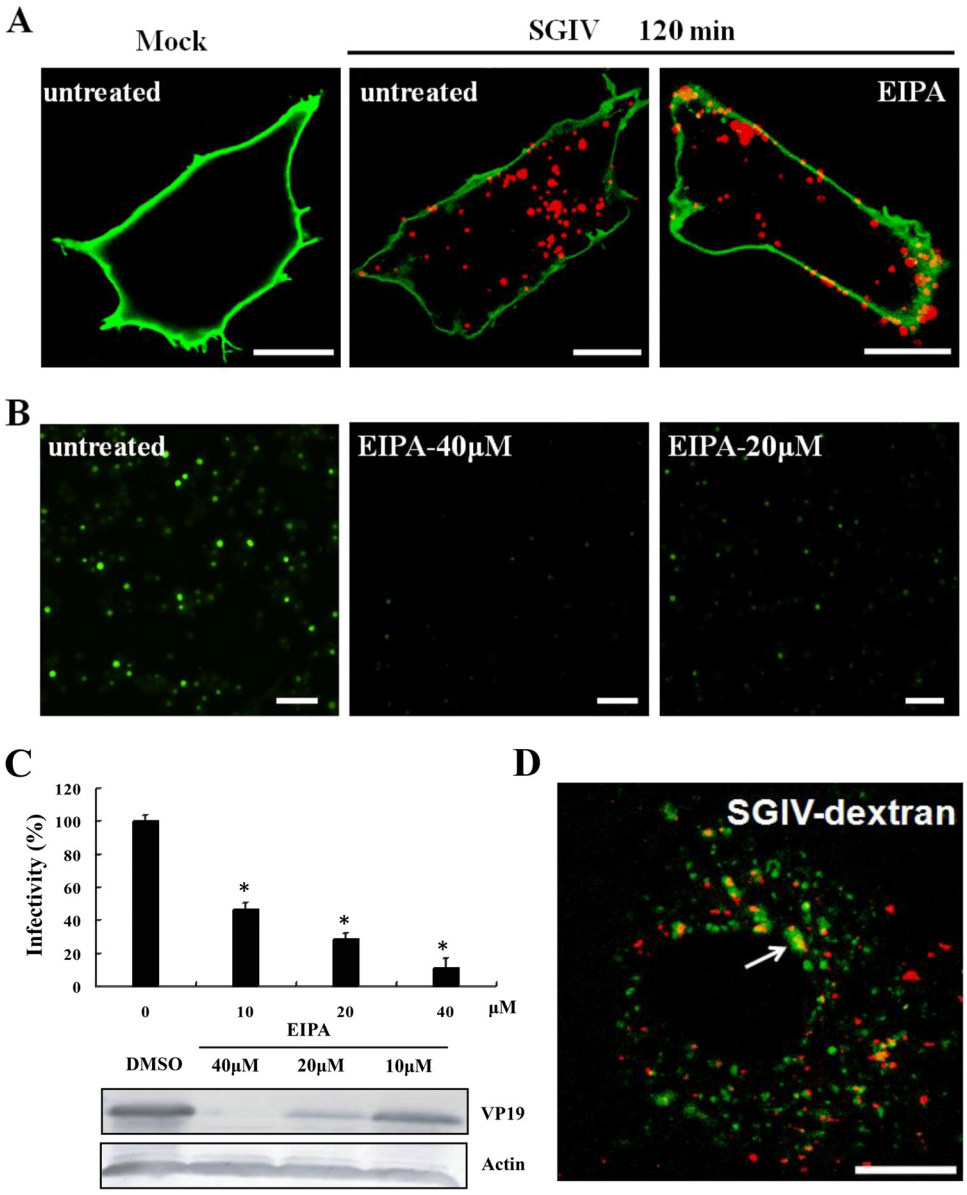

FIG 5 EIPA inhibits SGIV entry. (A) EIPA blocks SGIV uptake. Cells were pretreated with EIPA for 120 min and infected with Cy5-labeled SGIV for 120 min. After the infected cells were labeled with DiO (green), more than 100 cells were examined by CLSM. (B) VP19 expression was detected in mock-treated or EIPA-treated cells by IFA. GS cells were pretreated with different concentrations of EIPA for 120 min and then incubated with SGIV for 120 min. After being washed in citrate buffer to remove noninternalized viruses, the cells were collected at 48 hpi and detected by IFA. (C) EIPA impairs infectivity and viral protein synthesis. Infectivity was examined by IFA ($n = 3$; mean ± SD), and the levels of SGIV viral protein and β-actin were analyzed by Western blotting. *, $P < 0.05$. (D) Viral colocalization with dextran during SGIV infection. GS cells were infected with Cy5-labeled SGIV for 30 min, incubated with dextran for 25 min, and analyzed by CLSM. Arrow, dextran (green)-virus (red) colocalization. Scale bars are 10 μm (A and D) and 50 μm (B).

in the macropinocytic entry of virus particles (17). Activation of PAK1, the small GTPase Rac1, and a functional actomyosin network was shown to be essential for macropinocytosis during influenza virus entry (64), while EV1 and VACV entry via macropinocytosis depended on PAK1 and PKC (65, 66). In our study, the regulation of myosin II activity by phosphorylation of myosin light chain was inhibited by ML-7, and Rac1 activity was specifically inhibited by NSC23766, without affecting the closely related Rho-GTPases. We also used rottlerin and IPA-3 to inhibit PKC and PAK1 activities in GS cells, respectively. As shown in Fig. 6, ML-7 (Fig. 6A), NSC23766 (Fig. 6B), rottlerin (Fig. 6C), and IPA-3 (Fig. 6D) all significantly decreased the percentage of SGIV infection and reduced protein synthesis in a dose-dependent manner, as examined by IFA and Western blotting, suggesting that multiple signaling molecules were involved in SGIV entry. These data provide strong evidence to suggest that SGIV enters cells via the macropinocytosis pathway.

SGIV entry is pH dependent. Enveloped viruses such as influenza virus and VACV generally enter host cells by fusion with the plasma membrane, or via a low-pH endosomal route (67). However, endocytic entry of some viruses, including ISKNV, Epstein-Barr virus, and duck hepatitis B virus

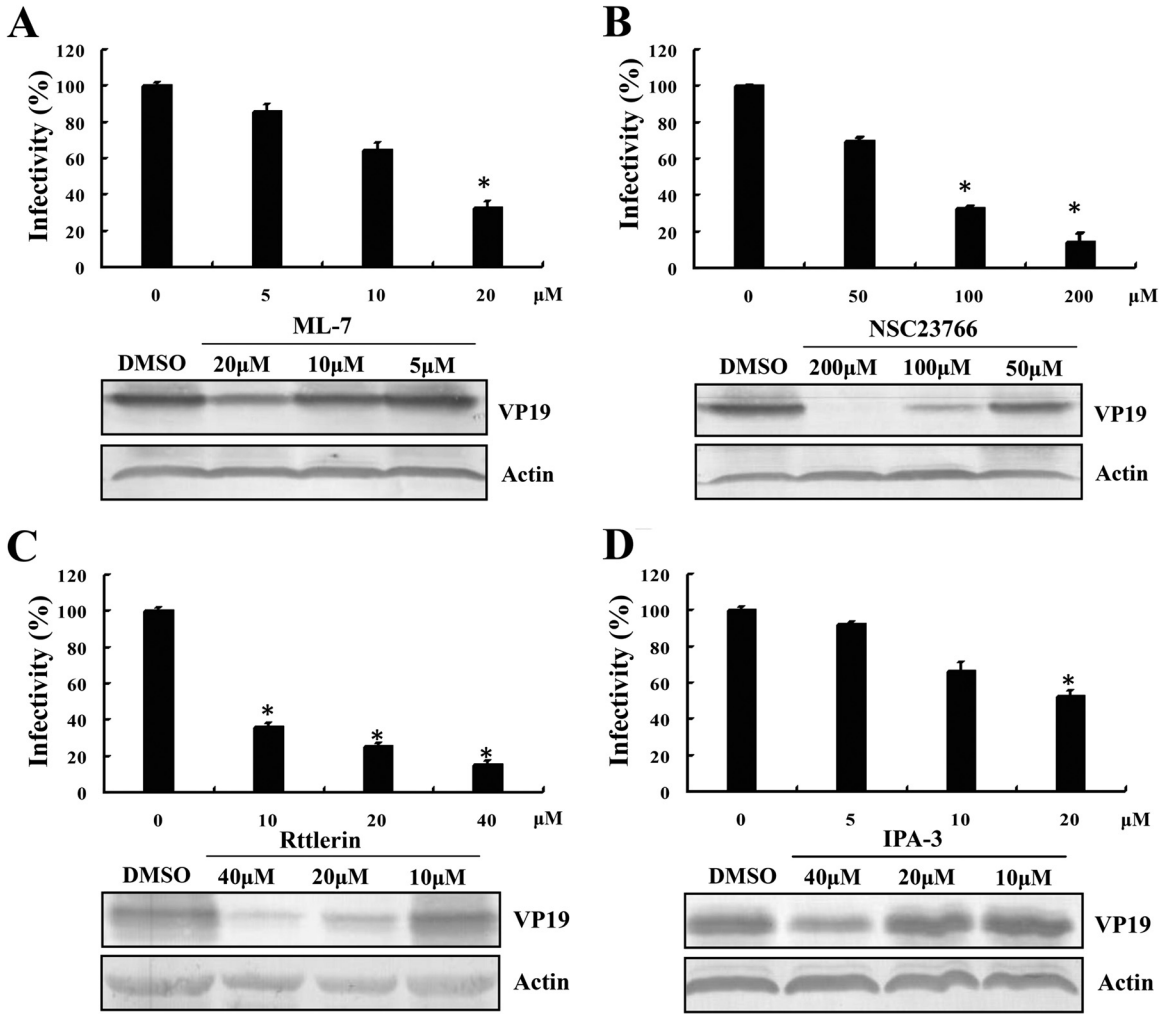

FIG 6 Roles of myosin II, Rac1, PKC, and PAK1 in SGIV infection. ML-7 (A), NSC23766 (B), rottlerin (C), and IPA-3 (D) reduced SGIV infectivity and viral protein synthesis. GS cells were pretreated with various concentrations of drugs for 120 min and then incubated with SGIV for 120 min. After being washed with citrate buffer to remove noninternalized viruses, the cells were collected at 48 hpi. IFA was performed to calculate the rate of SGIV infection ($n = 3$; mean ± SD), and the level of viral protein expression was detected by Western blotting. *, $P < 0.05$.

(DHBV), does not involve a pH-triggered step (49, 68, 69). To assess the role of low pH in SGIV infection, GS cells were pretreated with various concentrations of Baf A1 or CQ, which could inhibit the acidification of endosomes and LYs (70, 71). Both Baf A1 and CQ reduced SGIV infection, compared with that of mock-treated cells (Fig. 7A and B). Moreover, viral protein synthesis was strongly inhibited even in the presence of low concentrations of Baf A1 or CQ (Fig. 7A and B).

The endosome system, which could provide acidic compartments, usually plays a vital role in virus entry into host cells (72). During the endocytic process, virus particles trafficked from EEs to the LEs, followed by LYs (73). To determine if SGIV particles were tightly associated with the endosomes and LYs, we labeled EEs, LEs, and LYs by transfection with pEGFP-Rab5 and pEGFP-Rab7 and staining with LysoTracker, respectively. It was revealed that fluorescent SGIV particles colocalized and transported along with EEs, LEs, and LYs during the early stage of infection (Fig. 7C; see Movies S3 to S5 in the supplemental material). These results demonstrate that SGIV enters host cells in a pH-dependent manner.

SGIV entry into GS cells is dependent on the cytoskeleton. Upon internalization, viruses are usually delivered to endosomal compartments and transported to the nucleus along actin filaments/microtubules (74, 75). Live-cell imaging has shown that many viruses, such as HIV, influenza virus, and human adenovirus, travel along microtubules at speeds of several micrometers per second (2, 11, 76, 77), while PV and HBsAg show actin-dependent, microtubule-independent movements with high speeds (up to 5 μm/s) (2, 4, 44). To demonstrate the roles of microtubules/actin filaments during intracellular transport of SGIV, we detected the correlations between SGIV particles and microtubule/actin filaments. pEGFP-tub was transfected into GS cells to indicate microtubules, and Alexa Fluor 488 phalloidin was used to label actin filaments. Tracking of individual SGIV particles showed that the particles colocalized with actin filaments and microtubules (Fig. 8). At 30 min postinfection, numerous SGIV particles were located in the actin-rich protrusions extending from the cell surface, and several virus particles were observed on the same protrusion simultaneously (Fig. 8A). At 0.5 to 1 hpi, SGIV

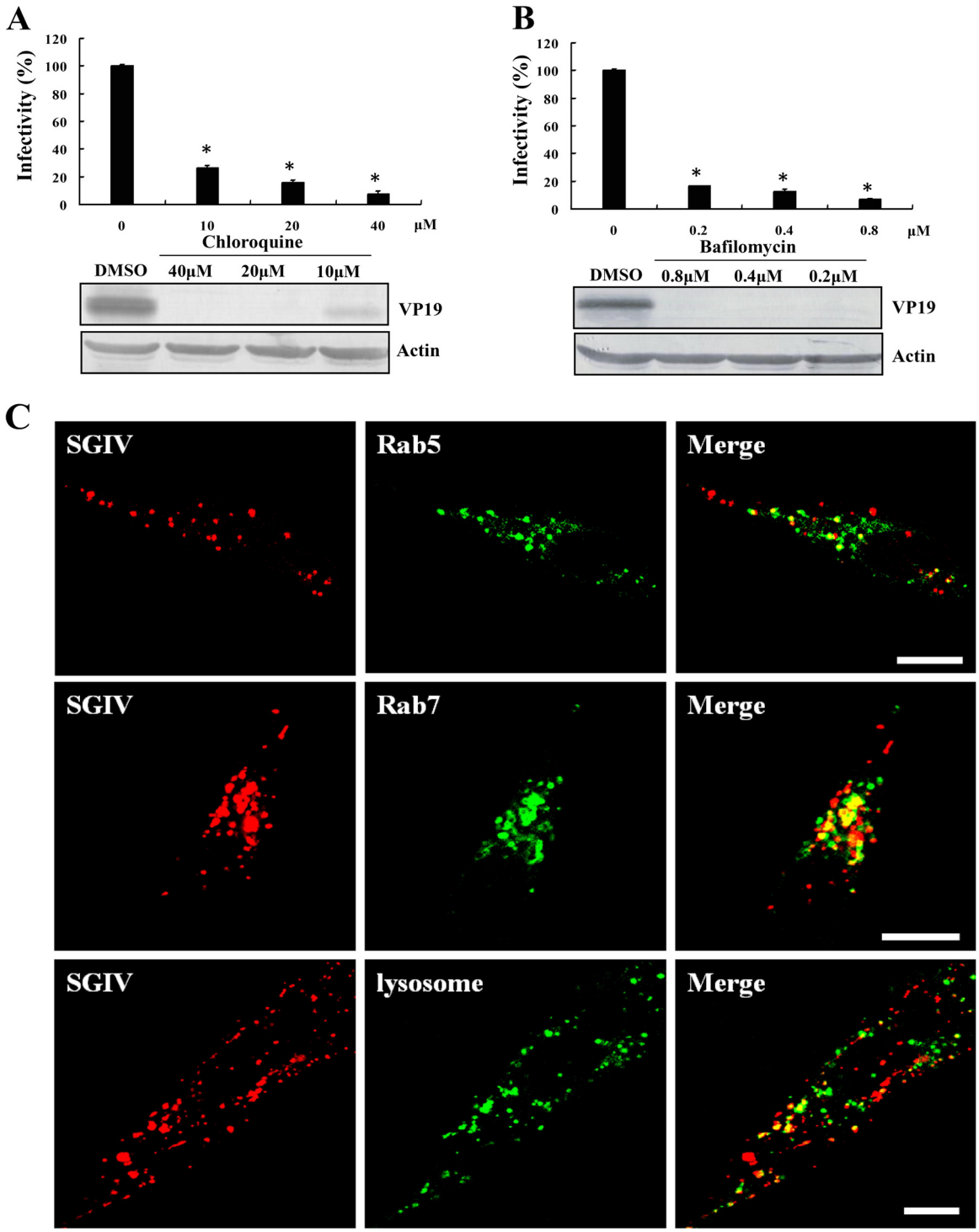

FIG 7 The low-pH endocytic pathway is required for SGIV infection. (A and B) Baf A1 and CQ reduce SGIV infectivity and viral protein synthesis. GS cells were pretreated with various concentrations of Baf A1 (A) and CQ (B) for 120 min and then incubated with SGIV for 120 min. After being washed with citrate buffer to remove noninternalized viruses, the cells were collected at 48 hpi. IFA was performed to calculate the rate of SGIV infection ($n = 3$; mean ± SD), and the level of viral protein expression was detected by Western blotting. *, $P < 0.05$. (C) SGIV particles are delivered to endocytic compartments during entry. After a 24-h posttransfection with pEGFP-Rab5 and pEGFP-Rab7, GS cells were infected with Cy5-labeled SGIV and immediately captured by CLSM. SGIV particles were observed with Rab5 and Rab7 at 30 and 60 min postinfection, respectively. Cells treated with LysoTracker after incubation with SGIV for 90 min were also observed, showing that SGIV particles were located in LYs. Scale bars are 10 μm.

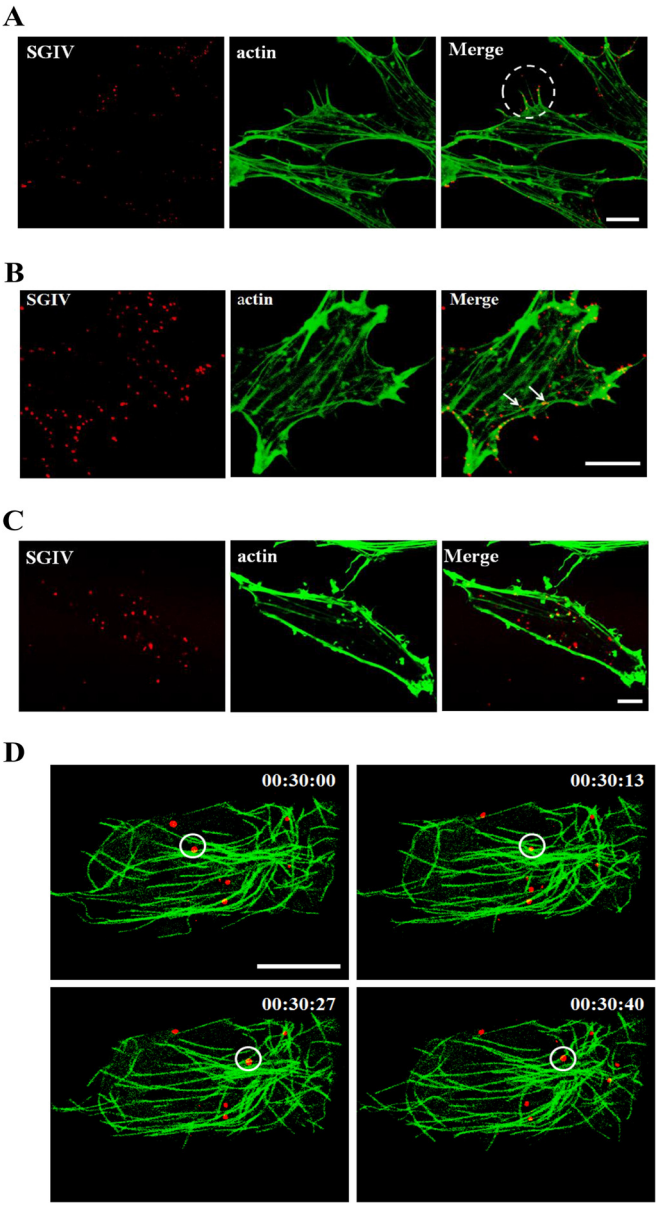

FIG 8 Colocalization of SGIV particles with cytoskeleton. (A to C) Detection of the colocalization between SGIV and actin. (A) SGIV binds to actin-rich protrusions. GS cells were infected with Cy5-labeled SGIV (red) at 28°C for 30 min, fixed, and stained for actin using Alexa Fluor 488 phalloidin (green) for 30 min. The dashed circle indicates more than one virus particle bound to a protrusion. (B) SGIVs are colocalized with actin filaments during the early stage of SGIV infection. The arrows show many virus particles (red) colocalized with actin filaments (green) near the cell membrane. (C) SGIV is located in dot-like actin filaments. GS cells were infected with Cy5-labeled SGIV at 28°C for 60 min, fixed, and stained for actin using Alexa Fluor 488 phalloidin for 30 min. (D) SGIV transport along microtubules. GS cells were transfected with pEGFP-tub (green) prior to infection. After 24 h, Cy5-labeled SGIV particles (red) were added to cells, and the images were captured immediately. Scale bars are 10 μm.

particles colocalized with dot-like actin and long actin filaments (Fig. 8B and C). In addition, SGIV particles were observed to move along microtubules during infection (Fig. 8D; see Movie S6 in the supplemental material), suggesting that both actin filaments and microtubules may be crucial for virus transport during infection.

To clarify the roles of actin filaments and microtubules during SGIV infection, the motility of SGIV particles was investigated after treatment with agents that depolymerized these cytoskeleton components. The trajectories of SGIV particles were extracted from digital images with a shortest-path tree algorithm, and the speeds calculated by two-dimensional data analysis of three-dimensional virus particle motion represented the lower bounds of the actual speeds (40). The motilities of individual SGIV particles in GS cells varied in control cells (Fig. 9A and B; see Movie S7 in the supplemental material), with the highest speed reaching 0.9 μm/s (Fig. 9C); some viruses were virtually static (arrow in Fig. 9B), while others showed directed movement covering several square micrometers (arrowhead in Fig. 9B). The motility of SGIV particles remained heterogeneous, but with relatively low speeds, after treatment with nocodazole, which depolymerizes microtubules by preventing the formation of one of the two interchain disulfide linkages (Fig. 9D to F; see Movie S8 in the supplemental material). In contrast, SGIV particles were mostly confined to a limited area with a speed of <0.4 μm/s after treatment with Cyto D, which inhibits actin filament elongation at the barbed end (Fig. 9G to I; see Movie S9 in the supplemental material). We also studied the motility of SGIV particles quantitatively. The percentages of SGIV trajectories with a peak speed of >0.05 μm/s were 30.4% in untreated cells, 10.6% in nocodazole-treated cells, and 12.8% in Cyto D-treated cells, indicating a significant reduction ($P < 0.05$) in the percentage of trajectories with a peak speed of >0.05 μm/s following treatment with nocodazole or Cyto D (Fig. 9J). We found similar results using 0.1, 0.15, 0.2, 0.25, and 0.3 μm/s as instantaneous threshold speeds, confirming that treatment with nocodazole and Cyto D reduced the motility of SGIV during infection. Mean-square displacement (MSD) analysis of particles showed that the average MSD was substantially reduced in nocodazole- and Cyto D-treated cells compared with untreated cells (Fig. 9K).

DISCUSSION

Viruses have evolved to exploit endocytosis as an effective means of entering host cells and being transported to sites suitable for replication. Knowledge of virus entry pathways is therefore important for understanding viral pathogenesis and developing effective drugs to block virus infection before entry, which represents the early, critical stage of infection. Iridoviruses are large DNA viruses that can infect cold-blooded vertebrates, invertebrates, crustaceans, and molluscs (78). The family *Iridoviridae* is currently composed of five genera: *Ranavirus*, *Lymphocystivirus*, *Megalocytivirus*, *Iridovirus*, and *Chloriridovirus*. Among these genera, ranaviruses have attracted much attention because of their impact on global ecological diversity and their role in heavy economic losses in the aquaculture industry (50, 79, 80). Although the events occurring during the early stage of ranavirus infection, especially virus entry, have been investigated, studies have been carried out only in nonhost cells (48, 49). Given that viruses can infect a wide variety of cell types and display different entry routines in different cells (81, 82), investigating the mechanism of entry into host cells is essential and critical for understanding the true behavior of ranavirus infection.

The well-characterized endocytic pathways exploited by viruses include clathrin-dependent and lipid raft/caveola-depen-

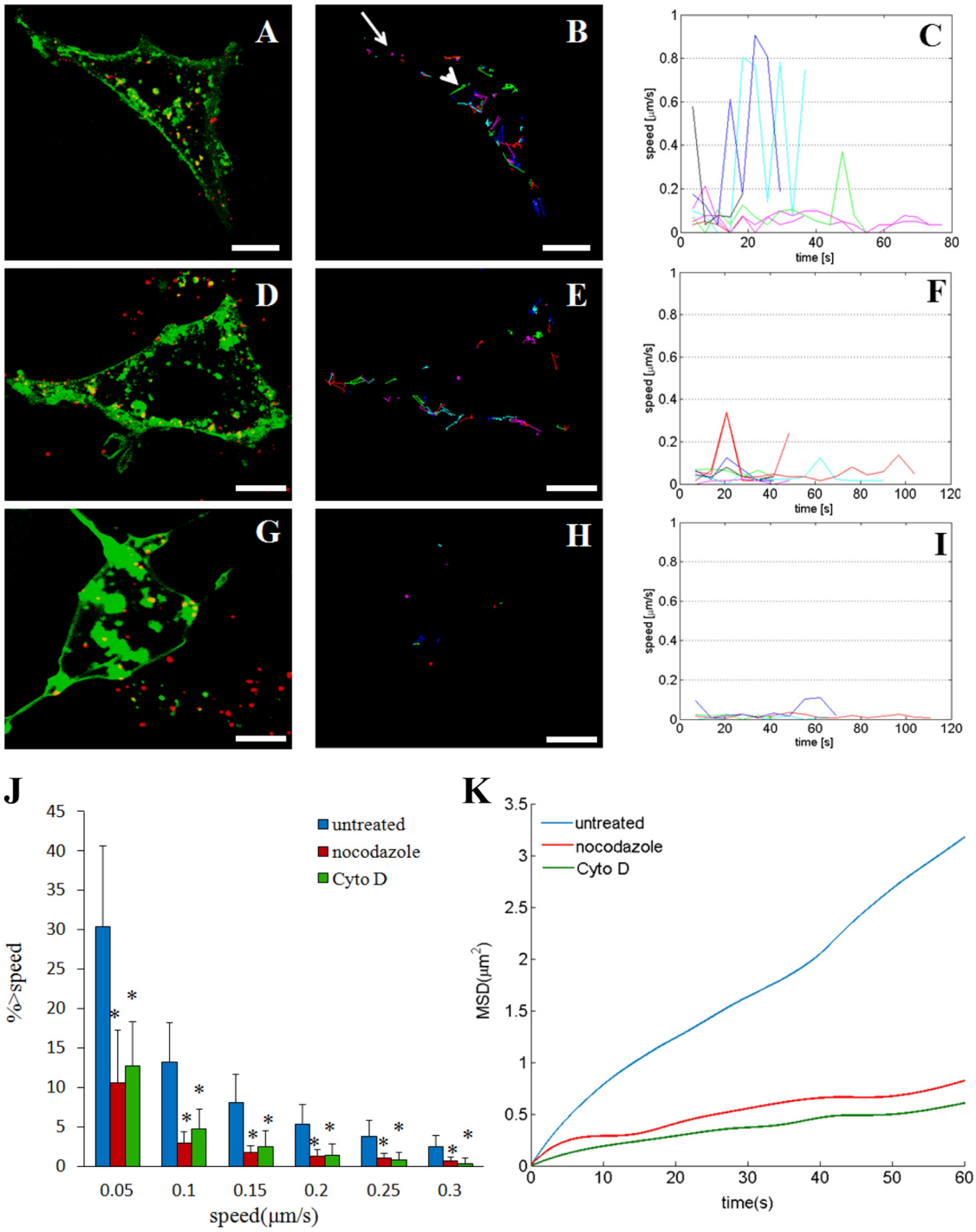

FIG 9 Motion of SGIV in untreated and nocodazole-treated or Cyto D-treated GS cells. (A to C) Motility of SGIV in untreated GS cells. (A) Confocal images of SGIV particles (red) in live cells labeled with DiO (green) (also shown in Movie S7 in the supplemental material). Representative trajectories (B) and their instantaneous speeds as a function of time (C) are also shown. The arrow in panel B indicates movement in a limited area, and the arrowhead indicates directed movement covering areas of several square micrometers. (D to F) Motility of SGIV in nocodazole-treated GS cells. GS cells were pretreated with 4 μM nocodazole for 2 h before infection with SGIV. (D) Confocal images of SGIV particles (red) in live cells labeled with DiO (green) (also shown in Movie S8 in the supplemental material). (E) Representative trajectories of SGIV particles. (F) Calculated instantaneous speeds of SGIV particles as a function of time. (G to I) Motility of SGIV in Cyto D-treated GS cells. GS cells were pretreated with 2 μM Cyto D for 1 h before infection with SGIV. (G) Confocal images of SGIV particles (red) in live cells labeled with DiO (green) (also shown in Movie S9 in the supplemental material). Representative trajectories of SGIV particles (H) and their instantaneous speeds as a function of time (I) are also shown. (J and K) Quantitative analysis of SGIV motion. (J) Comparison of SGIV motility with instantaneous speeds of >0.05, 0.1, 0.15, 0.2, 0.25, and 0.3 μm/s among untreated (blue bars), nocodazole-treated (red bars), and cytochalasin D-treated (green bars) cells. *, $P < 0.05$. More than 300 trajectories were analyzed. (K) MSD analysis of SGIV particles in untreated (blue line), nocodazole-treated (red line), and Cyto D-treated (green line) cells. Scale bars are 10 μm (A, B, D, and E) and 5 μm (G and H).

dent entry pathways (27). In clathrin-mediated endocytosis, clathrin is assembled on the inside face of the plasma membrane to form CCPs in response to virus infection. CPZ is known to inhibit clathrin-mediated endocytosis by preventing CCP assembly at the cell surface (9). Treatment with CPZ has revealed that several viruses enter cells via clathrin-mediated endocytosis, including HIV (83), hepatitis C virus (HCV) (84), ASFV (9), bovine ephemeral fever virus (BEFV) (10), HBV (85), rabies virus (86), and astrovirus (87). In our study, the percentage of SGIV-infected cells and viral protein synthesis were significantly and dose-dependently reduced by treatment with CPZ, while another inhibitor, hyperosmotic sucrose, which prevents clathrin and adapters from interacting (88), had a similar inhibitory effect on SGIV entry. Furthermore, after virus internalization, SGIV infection and viral protein synthesis were significantly inhibited by pretreating host cells with CQ or Baf A1, both of which are known to prevent endosome acidification. We therefore propose that SGIV enters host cells by clathrin-mediated endocytosis in a pH-dependent manner.

In addition to the inhibitory effect of clathrin-dependent pathway-specific inhibitors on SGIV entry, SGIV viral particles were also observed to colocalize with clathrin, Rab5, and Rab7 in host cells. Moreover, in accordance with a previous study showing that uptake by CCPs is a fast process relative to uptake by caveosomes (89), clathrin-mediated SGIV entry was relatively fast, compared with caveola-mediated endocytic entry of TFV and ISKNV (16, 49). These data thus consistently demonstrated that ranaviruses use clathrin-mediated endocytosis to enter host cells.

In contrast to clathrin-mediated endocytosis, caveolin-1 moves with caveola-derived vesicles to multiple interior compartments in the cytoplasm during caveola-dependent endocytosis. Because caveolae are rich in cholesterol and sphingolipids, caveola-mediated endocytosis is sensitive to cholesterol-depleting reagents such as filipin, nystatin, and MβCD (90). Some viruses, such as SV40 (91), TFV (49), ISKNV (16), EV1 (92), human HBV (93), MLV (94), coronavirus (95), and BK virus (96), enter cells via caveola-dependent, clathrin-independent endocytosis. However, our data revealed no reduction of SGIV infection by MβCD or nystatin, suggesting that lipid rafts and caveolae were not involved in SGIV entry and indicating that the caveola-mediated endocytosis is not a universal requirement for iridovirus entry into host cells.

The GTPase dynamin is a crucial element in the fission process of newly formed endocytic vesicles from the plasma membrane and is required for clathrin-mediated and lipid raft/caveola-based endocytosis (97–99). Many viruses, including rabies virus (86), BEFV (10), Rift Valley fever virus (100), and ASFV (9), have been shown to exploit the dynamin-dependent clathrin-mediated pathway to enter cells. Furthermore, some viruses enter cells via the dynamin-dependent caveola-mediated pathway, such as SV40 (101), Japanese encephalitis virus (102), TFV (49), and ISKNV (16). Dynasore is an effective dynamin inhibitor that can rapidly inhibit dynamin's GTPase activity and ultimately block dynamin-dependent endocytosis in cells (60). Using dynasore, we showed that inhibition of dynamin significantly decreased the percentage of SGIV infection and inhibited virus protein synthesis. Although infection by SGIV and that by another ranavirus, TFV, both depend on dynamin (49), the entry routines differ, suggesting that the mechanisms of iridovirus entry are complex.

In addition to clathrin-mediated, lipid raft/caveola-mediated entry, increased attention has recently been paid to the role of macropinocytosis in virus entry (17). The importance of Na^+/H^+ exchanger activity in macropinocytosis has led to use of the potent and specific Na^+/H^+ exchange inhibitor EIPA to evaluate the impact of macropinocytosis on virus entry (18). Macropinocytosis has been shown to be involved in the entry of many mammalian viruses, including EV1 (65), respiratory syncytial virus (103), filamentous influenza virus (104), EBOV (105), ASFV (19), VACV (66), and human cytomegalovirus (106). However, few studies have focused on the roles of macropinocytosis in fish virus entry (107). Our data showed that EIPA significantly inhibited SGIV entry and reduced viral protein synthesis. Moreover, SGIV particles were observed not only to bind to actin-rich protrusions extending from the cell surface but also to move to the cell surface by surfing along filopodia-like protrusions of GS cells or by protrusion retraction. Thus, we proposed that these protrusions may facilitate SGIV entry. In influenza virus-infected cells, actin-rich protrusions at the periphery of the cell can be stained by phalloidin and may result in the formation of macropinosomes (64). Furthermore, SGIV infection induced the uptake of dextran, which is a known marker of macropinocytosis/fluid-phase uptake, and numerous viral particles were colocalized with macropinosomes, suggesting a role for macropinocytosis in SGIV entry.

Several recent reports have demonstrated that certain signaling events are critical for defining the role of macropinocytosis in virus entry (17). Inhibitor analysis indicated that kinases such as PKC and PAK1, GTPase Rac1, and a functional actomyosin network were essential for macropinocytosis. As one of the most important kinases, PAK1 may be activated by Rac1, regulate cytoskeleton dynamics and motility, and be required during all stages of macropinocytosis (108). In our study, inhibition of PAK1 activity by IPA-3 or inhibition of Rac1 activity by NSC23766 significantly inhibited SGIV entry. In addition, inhibition of myosin II activity by ML-7 or inhibition of PKC activity by rottlerin also inhibited SGIV entry. Moreover, the inhibitory roles of these inhibitors were dose dependent, suggesting the involvement of multiple critical signaling molecules for macropinocytosis in SGIV entry. Based on these results, we propose that SGIV, similarly to EBOV, enters host cells via both macropinocytosis and clathrin-mediated endocytosis (109).

After internalization, viruses confront the issue of how to reach the site of replication, given that the size of viruses and the density of the cytoplasm prevent virus particles from reaching their desired destinations by free diffusion (41, 110). Viruses therefore hijack the host's cellular transport system, including microtubule- and actin-dependent transportation (4, 41, 44, 74, 110). Fluorescently labeled SGIVs colocalized with actin filaments and trafficked along microtubules in cells, suggesting that both actin filaments and microtubules may be involved in the movement of SGIV. Similarly, the cytoplasmic movement of influenza virus has also been shown to rely on both actin filaments and microtubules during different stages of infection (11).

It has been reported that viruses such as PV, adenovirus serotype 5, and HCV can move along actin filaments or microtubules at speeds of around 0.2 to 5.0 μm/s, similar to the speed of cellular particles (40, 75, 111, 112), which is much faster than the speeds achieved by random walking. In our study, the highest instantaneous velocity of SGIV particles measured was 0.9 μm/s, similar to that of infectious hematopoietic necrosis virus (IHNV) (113). Nocodazole or Cyto D/B can cause substantial inhibition of virus

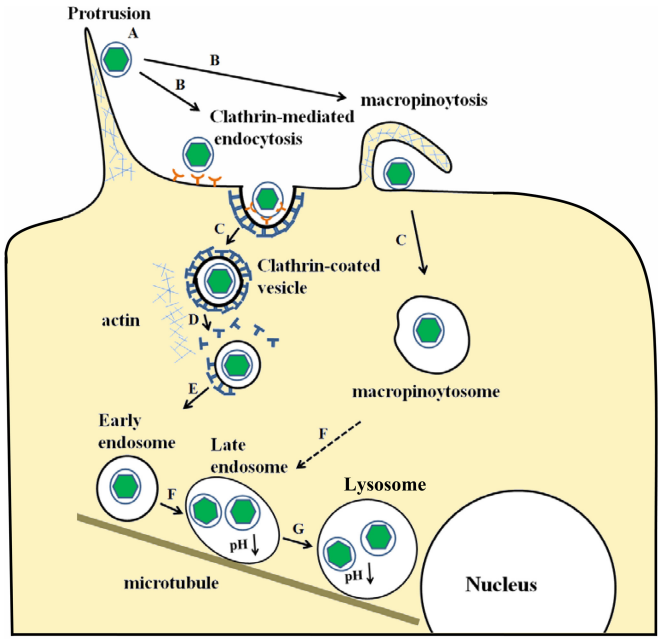

FIG 10 Model entry route of SGIV into GS cells. A, SGIV particles may transport along actin-rich protrusions to reach the cell surface. B, internalization of SGIV particles by clathrin-mediated endocytosis and macropinocytosis. C, internalized particles contained within CCVs and macropinosomes. D, CCVs containing individual SGIV particles are rapidly uncoated. E, the virus is transported to the EE. F, an EE matures into an LE by decreasing its pH, and the macropinosome may also undergo acidification. G, further acidification brings the LE to the LY. C and D may represent actin-dependent movement, while E, F, and G may represent microtubule-dependent movement.

motility in many viruses, including influenza virus (11), PV (40), and HBsAg (44). SGIV particles showed consistently lower instantaneous speeds in microtubule- or actin-deficient cells and were confined to a small area in cells lacking intact actin. Although we clarified that actin and microtubules were required for SGIV infection, whether the molecular motors, including myosins, kinesins, and dyneins, are involved in virus transport needs further investigation.

In conclusion, the evidence presented here demonstrates that SGIV enters host cells by clathrin-mediated endocytosis and macropinocytosis (Fig. 10). This process differs from caveola-mediated endocytosis, exploited by TFV or ISKNV, and clathrin-mediated endocytosis, demonstrated by FV3 (16, 48, 49). Once taken up by endocytosis, SGIV particles transport along actin filaments and microtubules in the cytoplasm. We propose that the ability of iridoviruses to initiate infection via multiple entry routes may be associated with their broad host range. In the case of mammalian viruses, bluetongue virus (BTV) can infect a wide variety of cell types in its mammalian host, and BTV-10 entry into Vero and HeLa cells occurs via clathrin-mediated endocytosis, while BTV-1 infection of BHK cells occurs via a clathrin-independent macropinocytosis-like entry mechanism (81, 82). Further studies are needed to determine the detailed mechanisms involved in the entry routes that iridoviruses use and the relevance of different entry pathways to virus pathogenesis.

ACKNOWLEDGMENTS

This work was supported by grants from the National Natural Science Foundation of China (31330082, 31172445, 21203177, and 21373200), the National Basic Research Program of China (973) (2012CB114402 and 2011CB933600), and the Knowledge Innovation Program of the Chinese Academy of Sciences (SQ201014).

REFERENCES

1. **Ruthardt N, Lamb DC, Bräuchle C.** 2011. Single-particle tracking as a quantitative microscopy-based approach to unravel cell entry mechanisms of viruses and pharmaceutical nanoparticles. Mol. Ther. **19:**1199–1211. http://dx.doi.org/10.1038/mt.2011.102.
2. **Sun E, He J, Zhuang X.** 2013. Live cell imaging of viral entry. Curr. Opin. Virol. **3:**34–43. http://dx.doi.org/10.1016/j.coviro.2013.01.005.
3. **Seisenberger G, Ried MU, Endress T, Büning H, Hallek M, Bräuchle C.** 2001. Real-time single-molecule imaging of the infection pathway of an adeno-associated virus. Science **294:**1929–1932. http://dx.doi.org/10.1126/science.1064103.
4. **Brandenburg B, Lee LY, Lakadamyali M, Rust MJ, Zhuang X, Hogle JM.** 2007. Imaging poliovirus entry in live cells. PLoS Biol. **5:**e183. http://dx.doi.org/10.1371/journal.pbio.0050183.
5. **Sieczkarski SB, Whittaker GR.** 2002. Dissecting virus entry via endocytosis. J. Gen. Virol. **83:**1535–1545.
6. **Marsh M, Helenius A.** 2006. Virus entry: open sesame. Cell **124:**729–740. http://dx.doi.org/10.1016/j.cell.2006.02.007.
7. **Doherty GJ, McMahon HT.** 2009. Mechanisms of endocytosis. Annu. Rev. Biochem. **78:**857–902. http://dx.doi.org/10.1146/annurev.biochem.78.081307.110540.
8. **Rust MJ, Lakadamyali M, Zhang F, Zhuang X.** 2004. Assembly of endocytic machinery around individual influenza viruses during viral entry. Nat. Struct. Mol. Biol. **11:**567–573. http://dx.doi.org/10.1038/nsmb769.
9. **Hernaez B, Alonso C.** 2010. Dynamin- and clathrin-dependent endocytosis in African swine fever virus entry. J. Virol. **84:**2100–2109. http://dx.doi.org/10.1128/JVI.01557-09.
10. **Cheng CY, Shih WL, Huang WR, Chi PI, Wu MH, Liu HJ.** 2012. Bovine ephemeral fever virus uses a clathrin-mediated and dynamin 2-dependent endocytosis pathway thatrequires Rab5 and Rab7 as well as microtubules. J. Virol. **86:**13653–13661. http://dx.doi.org/10.1128/JVI.01073-12.
11. **Lakadamyali M, Rust MJ, Babcock HP, Zhuang X.** 2003. Visualizing infection of individual influenza viruses. Proc. Natl. Acad. Sci. U. S. A. **100:**9280–9285. http://dx.doi.org/10.1073/pnas.0832269100.
12. **Johannsdottir HK, Mancini R, Kartenbeck J, Amato L, Helenius A.** 2009. Host cell factors and functions involved in vesicular stomatitis virus entry. J. Virol. **83:**440–453. http://dx.doi.org/10.1128/JVI.01864-08.
13. **Cureton DK, Harbison CE, Cocucci E, Parrish CR, Kirchhausen T.** 2012. Limited transferrin receptor clustering allows rapid diffusion of canine parvovirus into clathrin endocytic structures. J. Virol. **86:**5330–5340. http://dx.doi.org/10.1128/JVI.07194-11.
14. **van der Schaar HM, Rust MJ, Chen C, van der Ende-Metselaar H, Wilschut J, Zhuang X, Smit JM.** 2008. Dissecting the cell entry pathway of dengue virus by single-particle tracking in living cells. PLoS Pathog. **4:**e1000244. http://dx.doi.org/10.1371/journal.ppat.1000244.
15. **Kartenbeck J, Stukenbrok H, Helenius A.** 1989. Endocytosis of simian virus 40 into the endoplasmic reticulum. J. Cell Biol. **109:**2721–2729. http://dx.doi.org/10.1083/jcb.109.6.2721.
16. **Guo CJ, Wu YY, Yang LS, Yang XB, He J, Mi S, Jia KT, Weng SP, Yu XQ, He JG.** 2012. Infectious spleen and kidney necrosis virus (a fish iridovirus) enters Mandarin fish fry cells via caveola-dependent endocytosis. J. Virol. **86:**2621–2631. http://dx.doi.org/10.1128/JVI.06947-11.
17. **Mercer J, Helenius A.** 2009. Virus entry by macropinocytosis. Nat. Cell Biol. **11:**510–520. http://dx.doi.org/10.1038/ncb0509-510.
18. **Mercer J, Helenius A.** 2008. Vaccinia virus uses macropinocytosis and apoptotic mimicry to enter host cells. Science **320:**531–535. http://dx.doi.org/10.1126/science.1155164.
19. **Sánchez EG, Quintas A, Pérez-Núñez D, Nogal M, Barroso S, Carrascosa ÁL, Revilla Y.** 2012. African swine fever virus uses macropinocytosis to enter host cells. PLoS Pathog. **8:**e1002754. http://dx.doi.org/10.1371/journal.ppat.1002754.
20. **Amstutz B, Gastaldelli M, Kälin S, Imelli N, Boucke K, Wandeler E, Mercer J, Hemmi S, Greber UF.** 2008. Subversion of CtBP1-controlled macropinocytosis by human adenovirus serotype 3. EMBO J. **27:**956–969. http://dx.doi.org/10.1038/emboj.2008.38.
21. **Weed SA, Parsons JT.** 2001. Cortactin: coupling membrane dynamics to

cortical actin assembly. Oncogene **20:**6418–6434. http://dx.doi.org/10.1038/sj.onc.1204783.
22. **Charras GT, Hu CK, Coughlin M, Mitchison TJ.** 2006. Reassembly of contractile actin cortexin cell blebs. J. Cell Biol. **175:**477–490. http://dx.doi.org/10.1083/jcb.200602085.
23. **Kerr MC, Teasdale RD.** 2009. Defining macropinocytosis. Traffic **10:**364–371. http://dx.doi.org/10.1111/j.1600-0854.2009.00878.x.
24. **Haga Y, Miwa N, Jahangeer S, Okada T, Nakamura S.** 2009. CtBP1/BARS is an activator of phospholipase D1 necessary for agonist-induced macropinocytosis. EMBO J. **28:**1197–1207. http://dx.doi.org/10.1038/emboj.2009.78.
25. **Liberali P, Kakkonen E, Turacchio G, Valente C, Spaar A, Perinetti G, Böckmann RA, Corda D, Colanzi A, Marjomaki V, Luini A.** 2008. The closure of Pak1-dependent macropinosomes requires the phosphorylation of CtBP1/BARS. EMBO J. **27:**970–981. http://dx.doi.org/10.1038/emboj.2008.59.
26. **Saeed MF, Kolokoltsov AA, Albrecht T, Davey RA.** 2010. Cellular entry of Ebola virus involves uptake by a macropinocytosis-like mechanism and subsequent traffickingthrough early and late endosomes. PLoS Pathog. **6:**e1001110. http://dx.doi.org/10.1371/journal.ppat.1001110.
27. **Mercer J, Schelhaas M, Helenius A.** 2010. Virus entry by endocytosis. Annu. Rev. Biochem. **79:**803–833. http://dx.doi.org/10.1146/annurev-biochem-060208-104626.
28. **Sieczkarski SB, Whittaker GR.** 2002. Influenza virus can enter and infect cells in the absence of clathrin-mediated endocytosis. J. Virol. **76:**10455–10464. http://dx.doi.org/10.1128/JVI.76.20.10455-10464.2002.
29. **Gerondopoulos A, Jackson T, Monaghan P, Doyle N, Roberts LO.** 2010. Murine norovirus-1 cell entry is mediated through a non-clathrin-, non-caveolae-, dynamin- and cholesterol-dependent pathway. J. Gen. Virol. **91:**1428–1438. http://dx.doi.org/10.1099/vir.0.016717-0.
30. **Damm EM, Pelkmans L, Kartenbeck J, Mezzacasa A, Kurzchalia T, Helenius A.** 2005. Clathrin- and caveolin-1-independent endocytosis: entry of simian virus 40 into cells devoid of caveolae. J. Cell Biol. **168:**477–488. http://dx.doi.org/10.1083/jcb.200407113.
31. **Lehmann MJ, Sherer NM, Marks CB, Pypaert M, Mothes W.** 2005. Actin- and myosin-driven movement of viruses along filopodia precedes their entry into cells. J. Cell Biol. **170:**317–325. http://dx.doi.org/10.1083/jcb.200503059.
32. **Schelhaas M, Ewers H, Rajamäki ML, Day PM, Schiller JT, Helenius A.** 2008. Human papillomavirus type 16 entry: retrograde cell surface transport along actin-rich protrusions. PLoS Pathog. **4:**e1000148. http://dx.doi.org/10.1371/journal.ppat.1000148.
33. **ur Rehman Z, Sjollema KA, Kuipers J, Hoekstra D, Zuhorn IS.** 2012. Nonviral gene delivery vectors use syndecan-dependent transport mechanisms in filopodia to reach the cell surface. ACS Nano **6:**7521–7532. http://dx.doi.org/10.1021/nn3028562.
34. **Smith AE, Helenius A.** 2004. How viruses enter animal cells. Science **304:**237–242. http://dx.doi.org/10.1126/science.1094823.
35. **Gruenberg J.** 2009. Viruses and endosome membrane dynamics. Curr. Opin. Cell Biol. **21:**582–588. http://dx.doi.org/10.1016/j.ceb.2009.03.008.
36. **Sieczkarski SB, Whittaker GR.** 2003. Differential requirements of Rab5 and Rab7 for endocytosis of influenza and other enveloped viruses. Traffic **4:**333–343. http://dx.doi.org/10.1034/j.1600-0854.2003.00090.x.
37. **Kerr M, Teasdale RD.** 2014. Live imaging of endosome dynamics. Semin. Cell Dev. Biol. **31:**11–19. http://dx.doi.org/10.1016/j.semcdb.2014.03.027.
38. **Johns HL, Berryman S, Monaghan P, Belsham GJ, Jackson T.** 2009. A dominant-negative mutant of rab5 inhibits infection of cells by foot-and-mouth disease virus: implications for virus entry. J. Virol. **83:**6247–6256. http://dx.doi.org/10.1128/JVI.02460-08.
39. **Deinhardt K, Salinas S, Verastegui C, Watson R, Worth D, Hanrahan S, Bucci C, Schiavo G.** 2006. Rab5 and Rab7 control endocytic sorting along the axonal retrograde transport pathway. Neuron **52:**293–305. http://dx.doi.org/10.1016/j.neuron.2006.08.018.
40. **Vaughan JC, Brandenburg B, Hogle JM, Zhuang X.** 2009. Rapid actin-dependent viral motility in live cells. Biophys. J. **97:**1647–1656. http://dx.doi.org/10.1016/j.bpj.2009.07.011.
41. **Greber UF, Way M.** 2006. A superhighway to virus infection. Cell **124:**741–754. http://dx.doi.org/10.1016/j.cell.2006.02.018.
42. **Arhel N, Genovesio A, Kim KA, Miko S, Perret E, Olivo-Marin JC, Shorte S, Charneau P.** 2006. Quantitative four-dimensional tracking of cytoplasmic and nuclear HIV-1 complexes. Nat. Methods **3:**817–824. http://dx.doi.org/10.1038/nmeth928.
43. **Joo KI, Fang Y, Liu Y, Xiao L, Gu Z, Tai A, Lee CL, Tang Y, Wang P.** 2011. Enhanced real-time monitoring of adeno-associated virus trafficking by virus-quantum dot conjugates. ACS Nano **5:**3523–3535. http://dx.doi.org/10.1021/nn102651p.
44. **Hao X, Shang X, Wu J, Shan Y, Cai M, Jiang J, Huang Z, Tang Z, Wang H.** 2011. Single-particle tracking of hepatitis B virus-like vesicle entry into cells. Small **7:**1212–1218. http://dx.doi.org/10.1002/smll.201002020.
45. **Chinchar VG, Yu KH, Jancovich JK.** 2011. The molecular biology of frog virus 3 and other iridoviruses infecting cold-blooded vertebrates. Viruses **3:**1959–1985. http://dx.doi.org/10.3390/v3101959.
46. **Rothermel BB, Travis ER, Miller DL, Hill RL, McGuire JL, Yabsley MJ.** 2013. High occupancy of stream salamanders despite high ranavirus prevalence in a southern appalachians watershed. Ecohealth **10:**184–189. http://dx.doi.org/10.1007/s10393-013-0843-5.
47. **Chinchar VG, Waltzek TB.** 2014. Ranaviruses: not just for frogs. PLoS Pathog. **10:**e1003850. http://dx.doi.org/10.1371/journal.ppat.1003850.
48. **Braunwald J, Nonnenmacher H, Tripier-Darcy F.** 1985. Ultrastructural and biochemical study of frog virus 3 uptake by BHK-21 cells. J. Gen. Virol. **66:**283–293. http://dx.doi.org/10.1099/0022-1317-66-2-283.
49. **Guo CJ, Liu D, Wu YY, Yang XB, Yang LS, Mi S, Huang YX, Luo YW, Jia KT, Liu ZY, Chen WJ, Weng SP, Yu XQ, He JG.** 2011. Entry of tiger frog virus (an iridovirus) into HepG2 cells via a pH-dependent, atypical, caveola-mediatedendocytosis pathway. J. Virol. **85:**6416–6426. http://dx.doi.org/10.1128/JVI.01500-10.
50. **Qin QW, Lam TJ, Sin YM, Shen H, Chang SF, Ngoh GH, Chen CL.** 2001. Electron microscopic observations of a marine fish iridovirus isolated from brown-spotted grouper, Epinephelus tauvina. J. Virol. Methods **98:**17–24. http://dx.doi.org/10.1016/S0166-0934(01)00350-0.
51. **Gibson-Kueh S, Netto P, Ngoh-Lim GH, Chang SF, Ho LL, Qin QW, Chua FH, Ng ML, Ferguson HW.** 2003. The pathology of systemic iridoviral disease in fish. J. Comp. Pathol. **129:**111–119. http://dx.doi.org/10.1016/S0021-9975(03)00010-0.
52. **Song WJ, Qin QW, Qiu J, Huang CH, Wang F, Hew CL.** 2004. Functional genomics analysis of Singapore grouper iridovirus: complete sequence determination and proteomic analysis. J. Virol. **78:**12576–12590. http://dx.doi.org/10.1128/JVI.78.22.12576-12590.2004.
53. **Teng Y, Hou Z, Gong J, Liu H, Xie X, Zhang L, Chen X, Qin QW.** 2008. Whole-genome transcriptional profiles of a novel marine fish iridovirus, Singapore grouper iridovirus (SGIV) in virus-infected grouper spleen cell cultures and in orange-spotted grouper, Epinephulus coioides. Virology **377:**39–48. http://dx.doi.org/10.1016/j.virol.2008.04.011.
54. **Huang Y, Huang X, Yan Y, Cai J, Ouyang Z, Cui H, Wang P, Qin Q.** 2011. Transcriptome analysis of orange-spotted grouper (Epinephelus coioides) spleen in response to Singapore grouper iridovirus. BMC Genomics **556:**1471–2164. http://dx.doi.org/10.1186/1471-2164-12-556.
55. **Zhou S, Wan Q, Huang Y, Huang X, Cao J, Ye L, Lim TK, Lin Q, Qin Q.** 2011. Proteomic analysis of Singapore grouper iridovirus envelope proteins and characterization of a novel envelope protein VP088. Proteomics **11:**2236–2248. http://dx.doi.org/10.1002/pmic.200900820.
56. **Huang X, Huang Y, Ouyang Z, Xu L, Yan Y, Cui H, Han X, Qin Q.** 2011. Singapore grouper iridovirus,a large DNA virus, induces nonapoptotic cell death by a cell type dependent fashion and evokes ERK signaling. Apoptosis **16:**831–845. http://dx.doi.org/10.1007/s10495-011-0616-y.
57. **Huang X, Huang Y, Sun J, Han X, Qin Q.** 2009. Characterization of two grouper *Epinephelus akaara* cell lines: application to studies of Singapore grouper iridovirus (SGIV) propagation and virus-host interaction. Aquaculture **292:**172–179. http://dx.doi.org/10.1016/j.aquaculture.2009.04.019.
58. **Huang X, Gong J, Huang Y, Ouyang Z, Wang S, Chen X, Qin Q.** 2013. Characterization of an envelope gene VP19 from Singapore grouper iridovirus. Virol. J. **10:**354. http://dx.doi.org/10.1186/1743-422X-10-354.
59. **Martinez MG, Cordo SM, Candurra NA.** 2007. Characterization of Junin arenavirus cell entry. J. Gen. Virol. **88:**1776–1784. http://dx.doi.org/10.1099/vir.0.82808-0.
60. **Macia E, Ehrlich M, Massol R, Boucrot E, Brunner C, Kirchhausen T.** 2006. Dynasore, a cell-permeable inhibitor of dynamin. Dev. Cell **10:**839–850. http://dx.doi.org/10.1016/j.devcel.2006.04.002.
61. **Sánchez-San Martín C, López T, Arias CF, López S.** 2004. Characterization of rotavirus cell entry. J. Virol. **78:**2310–2318. http://dx.doi.org/10.1128/JVI.78.5.2310-2318.2004.
62. **Pietiäinen V, Marjomäki V, Upla P, Pelkmans L, Helenius A, Hyypiä T.** 2004. Echovirus 1 endocytosis into caveosomes requires lipid rafts,

dynamin II, and signaling events. Mol. Biol. Cell **15:**4911–4925. http://dx.doi.org/10.1091/mbc.E04-01-0070.
63. **Le Roux D, Le Bon A, Dumas A, Taleb K, Sachse M, Sikora R, Julithe M, Benmerah A, Bismuth G, Niedergang F.** 2012. Antigen stored in dendritic cells after macropinocytosis is released unprocessed from late endosomes to target B cells. Blood **119:**95–105. http://dx.doi.org/10.1182/blood-2011-02-336123.
64. **de Vries E, Tscherne DM, Wienholts MJ, Cobos-Jiménez V, Scholte F, García-Sastre A, Rottier PJ, de Haan CA.** 2011. Dissection of the influenza A virus endocytic routes reveals macropinocytosis as an alternative entry pathway. PLoS Pathog. **7:**e1001329. http://dx.doi.org/10.1371/journal.ppat.1001329.
65. **Krieger SE, Kim C, Zhang L, Marjomaki V, Bergelson JM.** 2013. Echovirus 1 entry into polarized Caco-2 cells depends on dynamin, cholesterol, and cellular factors associated with macropinocytosis. J. Virol. **87:**8884–8895. http://dx.doi.org/10.1128/JVI.03415-12.
66. **Schmidt FI, Bleck CK, Helenius A, Mercer J.** 2011. Vaccinia extracellular virions enter cells by macropinocytosis and acid-activated membrane rupture. EMBO J. **30:**3647–3661. http://dx.doi.org/10.1038/emboj.2011.245.
67. **Earp LJ, Delos SE, Park HE, White JM.** 2005. The many mechanisms of viral membrane fusion proteins. Curr. Top. Microbiol. Immunol. **285:**25–66.
68. **Köck J, Borst EM, Schlicht HJ.** 1996. Uptake of duck hepatitis B virus into hepatocytes occurs by endocytosis but does not require passage of the virus through an acidic intracellular compartment. J. Virol. **70:**5827–5831.
69. **Miller N, Hutt-Fletcher LM.** 1992. Epstein-Barr virus enters B cells and epithelial cells by different routes. J. Virol. **66:**3409–3414.
70. **Helenius A.** 2013. Virus entry: what has pH got to do with it? Nat. Cell Biol. **15:**125. http://dx.doi.org/10.1038/ncb2678.
71. **Bayer N, Schober D, Prchla E, Murphy RF, Blaas D, Fuchs R.** 1998. Effect of bafilomycin A1 and nocodazole on endocytic transport in HeLa cells: implications for viral uncoating and infection. J. Virol. **72:**9645–9655.
72. **Huotari J, Helenius A.** 2011. Endosome maturation. EMBO J. **30:**3481–3500. http://dx.doi.org/10.1038/emboj.2011.286.
73. **Suikkanen S, Sääjärvi K, Hirsimäki J, Välilehto O, Reunanen H, Vihinen-Ranta M, Vuento M.** 2002. Role of recycling endosomes and lysosomes in dynein-dependent entry of canine parvovirus. J. Virol. **76:**4401–4411. http://dx.doi.org/10.1128/JVI.76.9.4401-4411.2002.
74. **Döhner K, Sodeik B.** 2005. The role of the cytoskeleton during viral infection. Curr. Top. Microbiol. Immunol. **285:**67–108.
75. **Döhner K, Nagel CH, Sodeik B.** 2005. Viral stop-and-go along microtubules: taking a ride with dynein and kinesins. Trends Microbiol. **13:**320–327. http://dx.doi.org/10.1016/j.tim.2005.05.010.
76. **McDonald D, Vodicka MA, Lucero G, Svitkina TM, Borisy GG, Emerman M, Hope TJ.** 2002. Visualization of the intracellular behavior of HIV in living cells. J. Cell Biol. **159:**441–452. http://dx.doi.org/10.1083/jcb.200203150.
77. **Engelke MF, Burckhardt CJ, Morf MK, Greber UF.** 2011. The dynactin complex enhances the speed of microtubule-dependent motions of adenovirus both towards and away from the nucleus. Viruses **3:**233–253. http://dx.doi.org/10.3390/v3030233.
78. **Williams T, Barbosa-Solomieu V, Chinchar VG.** 2005. A decade of advances in iridovirus research. Adv. Virus Res. **65:**173–248. http://dx.doi.org/10.1016/S0065-3527(05)65006-3.
79. **Hoverman JT, Mihaljevic JR, Richgels KL, Kerby JL, Johnson PT.** 2012. Widespread co-occurrence of virulent pathogens within California amphibian communities. Ecohealth **9:**288–292. http://dx.doi.org/10.1007/s10393-012-0778-2.
80. **Schock DM, Ruthig GR, Collins JP, Kutz SJ, Carrière S, Gau RJ, Veitch AM, Larter NC, Tate DP, Guthrie G, Allaire DG, Popko RA.** 2010. Amphibian chytrid fungus and ranaviruses in the Northwest Territories, Canada. Dis. Aquat. Organ. **92:**231–240.
81. **Forzan M, Marsh M, Roy P.** 2007. Bluetongue virus entry into cells. J. Virol. **81:**4819–4827. http://dx.doi.org/10.1128/JVI.02284-06.
82. **Gold S, Monaghan P, Mertens P, Jackson TA.** 2010. Clathrin independent macropinocytosis-like entry mechanism used by bluetongue virus-1 during infection of BHK cells. PLoS One **5:**e11360. http://dx.doi.org/10.1371/journal.pone.0011360.
83. **Daecke J, Fackler OT, Dittmar MT, Kräusslich HG.** 2005. Involvement of clathrin-mediated endocytosis in human immunodeficiency virus type 1 entry. J. Virol. **79:**1581–1594. http://dx.doi.org/10.1128/JVI.79.3.1581-1594.2005.
84. **Blanchard E, Belouzard S, Goueslain L, Wakita T, Dubuisson J, Wychowski C, Rouillé Y.** 2006. Hepatitis C virus entry depends on clathrin-mediated endocytosis. J. Virol. **80:**6964–6972. http://dx.doi.org/10.1128/JVI.00024-06.
85. **Huang HC, Chen CC, Chang WC, Tao MH, Huang C.** 2012. Entry of hepatitis B virus into immortalized human primary hepatocytes by clathrin-dependent endocytosis. J. Virol. **86:**9443–9453. http://dx.doi.org/10.1128/JVI.00873-12.
86. **Piccinotti S, Kirchhausen T, Whelan SP.** 2013. Uptake of rabies virus into epithelial cells by clathrin-mediated endocytosis depends upon actin. J. Virol. **87:**11637–11647. http://dx.doi.org/10.1128/JVI.01648-13.
87. **Méndez E, Muñoz-Yañez C, Sánchez-San Martín C, Aguirre-Crespo G, Baños-Lara Mdel R, Gutierrez M, Espinosa R, Acevedo Y, Arias CF, López S.** 2014. Characterization of human astrovirus cell entry. J. Virol. **88:**2452–2460. http://dx.doi.org/10.1128/JVI.02908-13.
88. **Chen CL, Hou WH, Liu IH, Hsiao G, Huang SS, Huang JS.** 2009. Inhibitors of clathrin-dependent endocytosis enhance TGFbeta signaling and responses. J. Cell Sci. **122:**1863–1871. http://dx.doi.org/10.1242/jcs.038729.
89. **Nichols B.** 2003. Caveosomes and endocytosis of lipid rafts. J. Cell Sci. **116:**4707–4714. http://dx.doi.org/10.1242/jcs.00840.
90. **Nabi IR, Le PU.** 2003. Caveolae/raft-dependent endocytosis. J. Cell Biol. **161:**673–677. http://dx.doi.org/10.1083/jcb.200302028.
91. **Pelkmans L, Kartenbeck J, Helenius A.** 2001. Caveolar endocytosis of simian virus 40 reveals a new two-step vesicular-transport pathway to the ER. Nat. Cell Biol. **3:**473–483. http://dx.doi.org/10.1038/35074539.
92. **Marjomäki V, Pietiäinen V, Matilainen H, Upla P, Ivaska J, Nissinen L, Reunanen H, Huttunen P, Hyypiä T, Heino J.** 2002. Internalization of echovirus 1 in caveolae. J. Virol. **76:**1856–1865. http://dx.doi.org/10.1128/JVI.76.4.1856-1865.2002.
93. **Macovei A, Radulescu C, Lazar C, Petrescu S, Durantel D, Dwek RA, Zitzmann N, Nichita NB.** 2010. Hepatitis B virus requires intact caveolin-1 function for productive infection in HepaRG cells. J. Virol. **84:**243–253. http://dx.doi.org/10.1128/JVI.01207-09.
94. **Beer C, Andersen DS, Rojek A, Pedersen L.** 2005. Caveola-dependent endocytic entry of amphotropic murine leukemia virus. J. Virol. **79:**10776–10787. http://dx.doi.org/10.1128/JVI.79.16.10776-10787.2005.
95. **Nomura R, Kiyota A, Suzaki E, Kataoka K, Ohe Y, Miyamoto K, Senda T, Fujimoto T.** 2004. Human coronavirus 229E binds to CD13 in rafts and enters the cell through caveolae. J. Virol. **78:**8701–8708. http://dx.doi.org/10.1128/JVI.78.16.8701-8708.2004.
96. **Eash S, Querbes W, Atwood WJ.** 2004. Infection of Vero cells by BK virus is dependent on caveolae. J. Virol. **78:**11583–11590. http://dx.doi.org/10.1128/JVI.78.21.11583-11590.2004.
97. **Henley JR, Krueger EW, Oswald BJ, McNiven McNiven MA.** 1998. Dynamin-mediated internalization of caveolae. J. Cell Biol. **141:**85–99. http://dx.doi.org/10.1083/jcb.141.1.85.
98. **Sever S, Damke H, Schmid SL.** 2000. Dynamin: GTP controls the formation of constricted coated pits, the rate limiting step in clathrin-mediated endocytosis. J. Cell Biol. **150:**1137–1148. http://dx.doi.org/10.1083/jcb.150.5.1137.
99. **Roux A, Uyhazi K, Frost A, De Camilli P.** 2006. GTP-dependent twisting of dynamin implicates constriction and tension in membrane fission. Nature **441:**528–531. http://dx.doi.org/10.1038/nature04718.
100. **Harmon B, Schudel BR, Maar D, Kozina C, Ikegami T, Tseng CT, Negrete OA.** 2012. Rift Valley fever virus strain MP-12 enters mammalian host cells via caveola-mediated endocytosis. J. Virol. **86:**12954–12970. http://dx.doi.org/10.1128/JVI.02242-12.
101. **Pelkmans L, Püntener D, Helenius A.** 2002. Local actin polymerization and dynamin recruitment in SV40-induced internalization of caveolae. Science **296:**535–539. http://dx.doi.org/10.1126/science.1069784.
102. **Zhu YZ, Xu QQ, Wu DG, Ren H, Zhao P, Lao WG, Wang Y, Tao QY, Qian XJ, Wei YH, Cao MM, Qi ZT.** 2012. Japanese encephalitis virus enters rat neuroblastoma cells via a pH-dependent, dynamin and caveola-mediated endocytosis pathway. J. Virol. **86:**13407–13422. http://dx.doi.org/10.1128/JVI.00903-12.
103. **Krzyzaniak MA, Zumstein MT, Gerez JA, Picotti P, Helenius A.** 2013. Host cell entry of respiratory syncytial virus involves macropinocytosis followed by proteolytic activation of the F protein. PLoS Pathog. **9:**e1003309. http://dx.doi.org/10.1371/journal.ppat.1003309.
104. **Rossman JS, Leser GP, Lamb RA.** 2012. Filamentous influenza virus

enters cells via macropinocytosis. J. Virol. **86:**10950–10960. http://dx.doi.org/10.1128/JVI.05992-11.

105. **Nanbo A, Imai M, Watanabe S, Noda T, Takahashi K, Neumann G, Halfmann P, Kawaoka.** 2010. Ebolavirus is internalized into host cells via macropinocytosis in a viral glycoprotein-dependent manner. PLoS Pathog. **23:**e1001121. http://dx.doi.org/10.1371/journal.ppat.1001121.
106. **Haspot F, Lavault A, Sinzger C, Laib Sampaio K, Stierhof YD, Pilet P, Bressolette-Bodin C, Halary F.** 2012. Human cytomegalovirus entry into dendritic cells occurs via a macropinocytosis-like pathway in a pH-independent and cholesterol-dependent manner. PLoS One **7:**e34795. http://dx.doi.org/10.1371/journal.pone.0034795.
107. **Huang Y, Huang X, Ouyang Z, Wei S, Guo C, Qin Q.** 2014. Development of a new cell line from the snout of giant grouper, Epinephelus lanceolatus (Bloch), and its application in iridovirus and nodavirus pathogenesis. Aquaculture **432:**265–272. http://dx.doi.org/10.1016/j.aquaculture.2014.04.044.
108. **Dharmawardhane S, Schürmann A, Sells MA, Chernoff J, Schmid SL, Bokoch GM.** 2000. Regulation of macropinocytosis by p21-activated kinase-1. Mol. Biol. Cell **11:**3341–3352. http://dx.doi.org/10.1091/mbc.11.10.3341.
109. **Aleksandrowicz P, Marzi A, Biedenkopf N, Beimforde N, Becker S, Hoenen T, Feldmann H, Schnittler HJ.** 2011. Ebola virus enters host cells by macropinocytosis and clathrin-mediated endocytosis. J. Infect. Dis. **204**(Suppl 3)**:**S957–S967. http://dx.doi.org/10.1093/infdis/jir326.
110. **Sodeik B.** 2000. Mechanisms of viral transport in the cytoplasm. Trends Microbiol. **8:**465–472. http://dx.doi.org/10.1016/S0966-842X(00)01824-2.
111. **Leopold PL, Kreitzer G, Miyazawa N, Rempel S, Pfister KK, Rodriguez-Boulan E, Crystal RG.** 2000. Dynein- and microtubule-mediated translocation of adenovirus serotype 5 occurs after endosomal lysis. Hum. Gene Ther. **11:**151–165. http://dx.doi.org/10.1089/10430340050016238.
112. **Sampaio KL, Cavignac Y, Stierhof YD, Sinzger C.** 2005. Human cytomegalovirus labeled with green fluorescent protein for live analysis of intracellular particle movements. J. Virol. **79:**2754–2767. http://dx.doi.org/10.1128/JVI.79.5.2754-2767.2005.
113. **Liu H, Liu Y, Liu S, Pang DW, Xiao G.** 2011. Clathrin-mediated endocytosis in living host cells visualized through quantum dot labeling of infectious hematopoietic necrosis virus. J. Virol. **85:**6252–6262. http://dx.doi.org/10.1128/JVI.00109-11.